T.R.
BOLU ABANT İZZET BAYSAL UNIVERSITY
INSTITUTE OF GRADUATE STUDIES
Department of Chemistry

THE INFLUENCE OF SYNTHESIS CONDITIONS ON THE CRYSTAL STRUCTURE OF SOME NANOSIZED ZINC ORTHOBORATE MATERIALS

MASTER OF SCİENCE

MUHAMMED ÖZTÜRK

ACADEMIC SUPERVISOR
Prof. Dr. Ayşe MORKAN

BOLU, OCAK - 2023

APPROVAL OF THE THESIS

THE INFLUENCE OF SYNTHESIS CONDITIONS ON THE CRYSTAL STRUCTURE OF SOME NANOSIZED ZINC ORTHOBORATE MATERIALS submitted by **Muhammed ÖZTÜRK** and defended before the Examining Committe Members listed below in partial fulfillment of the requirements for the degree of **Master of Science** in **Department of Chemistry, Institute of Graduate Studies of Bolu Abant Izzet Baysal University in 5.01.2023** by

Examining Committee Members	**Signature**
Supervisor Prof. Dr. Ayşe MORKAN Bolu Abant İzzet Baysal University	.....
Member Prof. Dr. F. Devrim ÖZDEMİRHAN Bolu Abant İzzet Baysal University	.....
Member Assoc. Prof. Dr. Mecit AKSU Düzce University	.....

Prof. Dr. İbrahim KÜRTÜL

Director of Instıtute of Graduate Studies

ETHICAL DECLARATION

In this thesis dissertation that was properly prepared according to the Thesis Writing Rules of Bolu Abant İzzet Baysal University of the Institute of Graduates Studies, I hereby declare that;

- All data, information, and documents presented in the thesis were obtained in accordance with the academic and ethical rules,
- All data, documents, assessments, and results were presented in accordance with the scientific ethical and moral rules,
- All works that were benefitted in the thesis were appropriately cited,
- No alteration was made in the data used,
- Study presented in this thesis is original,

Otherwise, I declare that I accept the loss of all my rights in case any contradiction that may arise against me.

Based on the plagiarism report that was generated on the date of 01/02/2023 by using predetermined filtrations set by Directorate of Institute of Graduate Studies of the Turnitin programme, a plagiarism detection sofware, the similarity index detected was 22 %.

_____

Muhammed ÖZTÜRK

ABSTRACT

THE INFLUENCE OF SYNTHESIS CONDITIONS ON THE CRYSTAL STRUCTURE OF SOME NANOSIZED ZINC ORTHOBORATE MATERIALS
MSC THESIS
MUHAMMED ÖZTÜRK
BOLU ABANT IZZET BAYSAL UNIVERSITY
INSTITUTE OF GRADUATE STUDIES
DEPARTMENT OF CHEMISTRY
(SUPERVISOR: PROF. DR. AYŞE MORKAN)
BOLU, JANUARY 2023
xii + 61

In this present study, nanosized zinc orthoborate materials were successfully synthesized using various fuels (urea, glycine, tartaric acid, HMTA, citric acid, and β-Alanine) with starting materials, zinc (II) nitrate hexahydrate and boric acid by Solution Combustion Synthesis (SCS) method. The products were characterized using X-Ray Diffraction (XRD), Infrared spectroscopy (FTIR) and UV-VIS spectroscopy.
The effects of different fuels and temperatures (400-900^{o}C) on the structural properties of synthesized products were analyzed using XRD technique. Examining XRD data, the alpha-$Zn_3B_2O_6$ as triclinic was detected at 600^{o}C for all fuels except glycine fuel. The transformation of alpha phase to beta-$Zn_3B_2O_6$ as monoclinic was observed at 700^{o}C and higher temperatures. The particle size of the synthesized alpha and beta form of zinc orthoborates were found in nano scale through the calculation of XRD data by Debye-Scherrer's equation. Due to these calculations, the crystallite sizes of the alpha zinc orthoborates were found in the range of 14-24 nm whereas beta zinc orthoborates between 22-31 nm.
Analyzing the FTIR data, the bending of BO_3 vibration at 695-720 cm^{-1}, symmetric stretching BO_3 vibrations at 1010-1065 cm^{-1} and asymmetric stretching BO_3 vibrations at 1220-1245 cm^{-1} were detected as the characteristic bands of zinc orthoborates.
Optical properties of the products were investigated by diffuse reflectance spectroscopy, DRS measurements. The absorbance and reflectance spectra were assigned between 200-900 nm. At 600^{o}C and 700^{o}C the spectra of all synthesized products with different fuels are observed in blue shift in order of citric acid, HMTA, urea, tartaric acid, glycine and beta-alanine.

KEYWORDS: Solution Combustion Synthesis (SCS), zinc orthoborate, nanosized, XRD, FTIR.

ÖZET

SENTEZ KOŞULLARININ BAZI NANO BOYUTLU ÇİNKO ORTOBORAT MALZEMELERİN KRİSTAL YAPILARI ÜZERİNDEKİ ETKİSİ
YÜKSEK LİSANS TEZİ
MUHAMMED ÖZTÜRK
BOLU ABANT İZZET BAYSAL ÜNİVERSİTESİ
LİSANSÜSTÜ EĞİTİM ENSTİTÜSÜ
KİMYA ANABİLİM DALI
(TEZ DANIŞMANI: PROF.DR.AYŞE MORKAN
BOLU, OCAK - 2023
xii + 61

Bu çalışmada, nanoboyutlu çinko ortoborat malzemeleri, çeşitli yakıtlar (üre, glisin, tartarik asit, HMTA, sitrik asit ve β-Alanin) ile çinko (II) nitrat hekzahidrat ve borik asit başlangıç maddeleri, kullanılarak Çözeltide Yanma Sentez yöntemi (SCS) ile başarıyla sentezlendi. Ürünler, X-Işını Kırınımı (XRD), Kızılötesi spektroskopi (FTIR) ve UV-VIS spektroskopisi kullanılarak karakterize edildi.

Farklı yakıt ve sıcaklıkların (400-900^{o}C) sentezlenen ürünlerin yapısal özellikleri üzerindeki etkileri XRD tekniği kullanılarak analiz edildi. XRD verileri incelendiğinde, glisin yakıtı dışındaki tüm yakıtlar için 600^{o}C'de triklinik alfa-$Zn_3B_2O_6$ tespit edilmiştir. Alfa fazının monoklinik beta-$Zn_3B_2O_6$'ya dönüşümü 700^{o}C ve daha yüksek sıcaklıklarda gözlendi. Sentezlenen çinko ortoboratların alfa ve beta formlarının parçacık büyüklükleri, XRD verilerinin Debye-Scherrer denklemi ile hesaplanmasıyla nano ölçekte bulunmuştur. Bu hesaplamalar sonucunda alfa çinko ortoboratların kristalit boyutları 14-24 nm aralığında, beta çinko ortoboratların ise 22-31 nm aralığında bulunmuştur.

FTIR verileri incelendiğinde, çinko ortoboratların karakteristik bantları olarak 695-720 cm^{-1}'de BO_3 titreşiminin bükülmesi, 1010-1065 cm^{-1}'de simetrik esneme BO_3 titreşimleri ve 1220-1245 cm^{-1}'de asimetrik esneme BO_3 titreşimleri tespit edildi.

Ürünlerin optik özellikleri, dağınık yansıma spektroskopisi, DRS ölçümleri ile incelenmiştir. Absorbans ve yansıma spektrumları 200-900 nm arasında belirlenmiştir. 600^{o}C ve 700^{o}C'de farklı yakıtlarla sentezlenen tüm ürünlerin spektrumlarında, sitrik asit, HMTA, üre, tartarik asit, glisin ve beta-alanin sırasıyla, maviye kayma gözlenmiştir.

ANAHTAR KELİMELER: Çözeltide Yanma Sentezi (SCS), çinko ortoborat nano boyut, XRD, FTIR.

TABLE OF CONTENTS

Page

LIST OF FIGURES

Page

LIST OF TABLES

Page

LIST OF PICTURES

Page

LIST OF ABBREVIATIONS AND SYMBOLS

CA	**:** Citric Acid
TA	**:** Tartaric Acid
HMTA	**:** Hexamethylenetetramine
GLY	**:** Glycine
U	**:** Urea
B-AL	**:** Beta-Alanine
FT-IR	**:** Fourier Transform Infrared
XRD	**:** X-Ray Diffraction
UV-VIS	**:** Ultraviolet-Visible
SCS	**:** Solution Combustion Synthesis
ICDD	**:** International Center for Diffraction Data
DRS	**:** Diffuse Reflectance Spectroscopy

ACKNOWLEDGEMENTS

I would like to express my deepest gratitude thanks to my supervisor, **Prof. Dr. AYŞE MORKAN** for her great guidance, honest advice, valuable criticism, continuous encouragements and insight throughout my master's studies.

I would like to send my deepest appreciation to Liska FADLIYANI for her assistance and support during my research.

I am very thankful to Gülden ÖZEN KAHVECİ for X-Ray studies.

I would also like to express my sincere gratitude to my family for their love, encouragement, and support during my thesis.

1. INTRODUCTION

Borax was known in ancient times for its use in the preparation of glazes hard glass and glazes. Some research was accomplished in the 18th century, and Davy, Gay Lussac and Thenard pioneered the purification of impure boron in 1808. H. Moisson obtained samples with 95-98% purity with a reduction of Mg. A product of the last century is high-purity boron. In the past few decades, it has been found that various crystal structures react with most metals, oxygen, and nitrogen at high temperatures and that their elemental nature is not easily degraded. The given name boron was suggested by Davy to interpret the element's resource (1).

It is known that the amount of boron in volcanic gases and hot spring waters is high, and even reaches economic concentrations in some places. The amount of boron in hot spring waters in the regions where boron deposits are located in Turkey and America is over 100 ppm. Most of the researchers connect the source of boron to magma (2).

According to the distribution of boron in various rocks, it is seen that the boron content in marine sediments is higher than in igneous rocks. The amount of boron that marine sediments take from sea water is higher than the amount of boron in the sea (2).

1.1 BORON

Boron is the 5^{th} elemen in the periodic table that has the relative atomic mass and atomic number as 10.81 amu and 5, respectively. Boron is found in the group IIIA in the periodic table which is a semiconductor and semi-metal. Boron element is in the 13th group of the periodic table. It has two different stable isotopes which are ^{10}B and ^{11}B, which are distributed in nature as 19.1%-20.3% and 79.7-80.9%, respectively. Boron has greater ionization energies (Table 1.2) compare to the other elements of the III-A group (3).

It is found in nature in two forms, crystalline and amorphous. The intensity of amorphous boron is 2.34 g/cm^3 and the crystal boron density is 2.33 g/cm^3. It is black in color and has a melting point around 2300 ºC. It also has visible point of 2550 ºC and have a width between metal and non-metal (4).

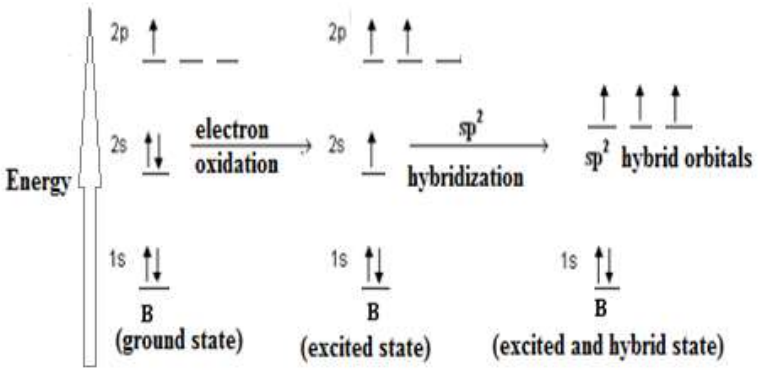

Figure 1.1. sp^2 hybridization of boron

In optical properties, the crystalline type of boron is like to diamond and is nearly as hard as diamond. Elemental boron is a black monoclinic crystal at solid at room temperature. It finds as brown or yellow amorphous powder in the impure solid form. Though crysta boron is very harsh, it is easily broken because its a metalloid, which shows between nonmetal and metal elements (4).

Conversely, the elements show several resemblances to their nonmetal neighbors, silicon and carbon, similar in a prominent tendency to create molecular and covalent compounds, but it differs strongly from them due to its electron deficiency that contains one missing valence electron (5).

Figure 1.2. Elemental boron appearance

Earth's crust (Lithosphere) includes approximately 0.0003% boron. The majority found that Boron is the 51st element in the earth's crust. In nature, boron

is known to have about 230 types of boron minerals (5). The physical properties of boron element are summarized in Table 1.1.

Table 1.1. Physical properties of boron element

Physical state (20 °C, 1 atm)	Solid
Appearance	Yellow-Brown nonmetallic crystal
Melting point	2300 °C
Boilin point	4002 °C
Heat of vaporization	489 kJ/mol
Heat capacity	11,087 J/mol.K
Specific heat	1.027 J/g.K.
Density	2.34 g/cm^3
Thermal conductivity	0.274 W/cm.K
Electrical conductivity	1.0 E^{-12} 10^6/cm.Ω
Coefficient of thermal expansion	0.0000083 1/ °C
Hardness	9.3 Mohs
Atomization enthalpy	573 kJ/mol (25 °C)
Evaporation enthalpy	480 kJ/mol
Molar volume	4.69 cm^3/mol
Vapor pressure	0.348 Pa
Fusion enthalpy	22.18 kJ/mol
Elastic modulus	320/GPa

Although the boron ingredient in the soil is generally 10-20 ppm, the high level concentrations of boron are found in the region from the Mediterranean to Kazakhstan and in the the western regions of the USA. It is discover in the marine

water, 0.5-9.6 ppm and 0.01-1.5 ppm in freshwater. Economically sized and high concentration boron deposits are mostly arid, volcanic and hydrothermal activity of the USA and Turkey, as the oxygen-bound compounds of boron located in the regions (5).

The chemical properties of boron bound up with grain size and structure, it is known that the boron crystal does not react readily while the small particle size boron reacts easily. It forms boric acid and other products when its allow to react with water at high temperatures. It does not deteriorate when boiled with hydrochloric and hydrofluoric acids. Very finely ground boron is slowly oxidized if treated with concentrated nitrate acid. Its reaction with mineral acids is explosive or slow based on the temperature and concentration. On the other hand, Boric Acid is formed as an intermediate product. It is difficult to obtain pure boron element and boron with 95-98% purity. It amorphous form was obtained by the decrease of boric oxide with magnesium and filtered by washing the impurity with base and acid. The resulting boron contains compounds containing oxide and boron and is dark brown in the form of small crystals (6).

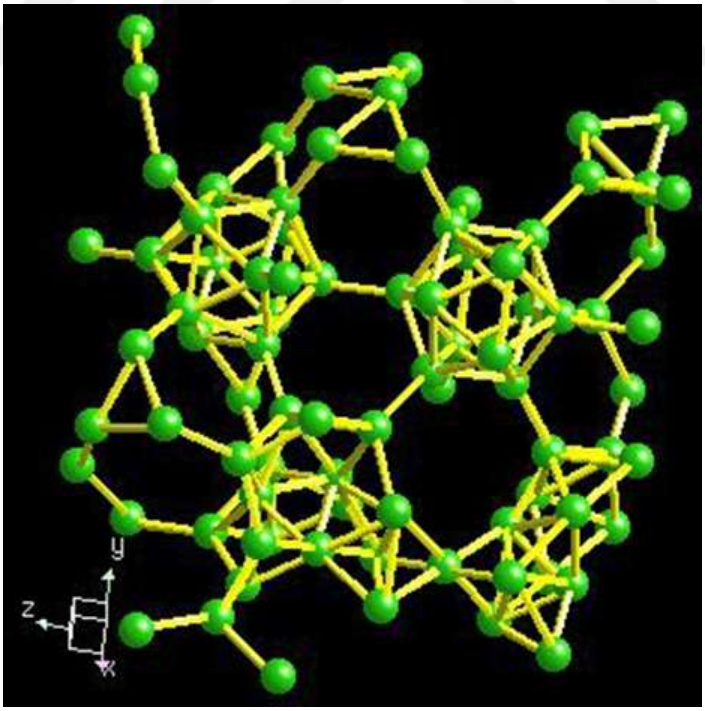

Figure 1.3. Crystal structure of boron (9)

The atomic and chemical properties of boron are summarized in Table 1.2

Table 1.2. Atomic and chemical properties of boron

Atomic diameter	1.17 Å
Atomic volume	4,6 cm^3/mol
Ionic diameter	0.23 Å
Electron configuration	$1s^2\ 2s^2p^1$
Crystal structure	Rhombohedral
Valence electrons	$2s^2p^1$
Number of neutrons	6
Number of protons	5
Number of electrons	5
Heat of fusion	50.2 kJ/mol
Electronegativity (Pauling)	2.04
Valence electron potential (-eV)	190
Electrochemical equivalent	0.1344 g/amp.hr
Ionization potential	First:8,298 Second:25,154 Third: 37.93

1.1.1. History of Boron

Boron mineral is one of the most interesting minerals in the world in terms of its versatile uses as well as having economic value and has been drawn great attentions for many years. It is known that boron salts were first used in gold mining in Tibet 4000 years ago. It is estimated that borax was first used by the Babylonians 4000 years ago in gold processing and various purposes, as it increased fluidity. It has been determined that the Egyptians used it in medicine, metallurgy, and pipe mummification. Glaze material in ceramics with the discoveries made over time. It has been used as a cleaning agent and as a therapeutic germicidal (7).

The ancient Greeks and Romans used borates as a cleaning agent, and the Arabs Used them once as medicine. Boric acid was made from borax in the early 1700s. In 1702, Hommerg first obtained boric acid by heating borax with iron sulfate. Elemental boron was fabricated in the early 1800s (7). Boron element was decomposed in 1808 by Louis Jacques Thernad and Joseph Louis Gay-Lussac and alone by Sir Humphry Davy by heating boric acid with potassium. The impure, amorphous brownish-black powder produced by this method remained the purest known form of boron for more than a century. The modern boron industry begins with the introduction of boron from Tibet to Europe in the 13th century (7).

In 1771, it was discovered that Sassolite was found in hot springs in Tuscany, Italy. Boric acid manufacture started in Italy in 1830. In the identical period, the first industrial borax mining started in Chile in 1852. Later, with the discovery and operation of the deposits in Nevada, California, Calico Moutain, and Kramer regions, the USA became the first country to meet the world's boron requirement (8). Colemanite deposits were found in Bigadiç in 1950 and Mustafa Kemal Paşa region in 1952.With the discovery and operation of starting Kütahya Emet Kolemanit in 1956 and Eskişehir Kırka Borax deposits in 1961, Turkey rised its share in world boron manufacture from 3% to 15% in 1962 and to 39% in 1977 (9).

1.1.2. Boron Minerals and Reserves

The inorganic borates are known as minerals since elemental boron are could not be found as pure form on Earth and there are almost 250 diverse types of boron compounds which composed of inorganic borates. Boron minerals, usually, obtain and be formed of earth alkali and alkali metals such as Na, Mg, and Ca. Boron minerals take names following the ratio of metals in their compounds, the aqueous ingredient, and crystal structure (11).

Borax has been used in advance of the end of the eighteenth century. The new resources of borax were invented and explored at the beginning of the 19th century. Borax is found in nature as a mineral associated with clay and other impurities. Boron minerals are minerals that include boron oxide (B_2O_3) in distinct proportions in their structures. Although there are a wide variety of minerals of boron in nature, commercially significant boron minerals; are kernite, hydroboracite, ulexite, tincal, probertite, boracite, pandermite, and syzabelite (2).

Since the general properties of boron products based on the quantity of B_2O_3, different boron products have properties to be used interchangeably. Boron minerals, according to the chemical composition of the deposits; strontium borates, silicon-calcium borates, alkali metal borates, transition metal borates, calcium borates, sodium-calcium borates, sodium borates, magnesium-calcium borates, magnesium borates ammonium borates, complex borates (2).

Some boron minerals with commercial residues and their boron oxide (B_2O_3) percentages are shown in Table 1.3.

Table 1.3. Some commercially important boron minerals(13)

Minerals	Formula
Inyoite	$Ca_2B_6O_{11}.\ 13H_2O$
Pandermite	$Ca_4B_{10}O_{19}.7H_2O$
Inderite	$Mg_2B_6O_{11}.15H_2O$
Hydroboracite	$CaMgB_6O_{11}.6H_2O$
Boracite	$Mg_3B_7O_{13}Cl$
Ascharite	$Mg_2B_2O_5.H_2O$
Datolite	$Ca_2B_2Si_2O_9.H_2O$
Kernite	$Na_2B_40_7.4H_2O$
Tincalconite	$Na_2B_40_7.5H_2O$
Tincal	$Na_2B_40_7.10H_2O$
Probertite	$NaCaB_50_9.5H_2O$
Ulexite	$NaCaB_50_9.8H_2O$
Colemanite	$Ca_2B_6O_{11}.5H_2O$
Meyerhofferite	$Ca_2B_6O_{11}.7H_2O$
Sassolite (natural boric acid)	H_3BO_3

Boron minerals can be categorized according to their chemical structures as borates containing boric acid, borofluorites, crystalline water, anhydrous borates, borosilicate minerals, compound borates, and non-borates. According to boron

compound products, they are classified as refined boron products, crude boron products, and boron end products (11).

Table 1.4. Common Used Boron Minerals

Mineral	**Empirical Formula**	**B_2O_3 content, wt%**	**Location of minerals**
Colemanite	$Ca_2B_6O_{11}.5H_2O$	50.8	Turkey
Suanite	$Mg_2B_2O_5$	46.3	China
Ulexite	$NaCaB_5O_9.8H_2O$	43.0	South America, Turkey
Borax	$Na_2B_4O_7.10H_2O$	36.5	Turkey, United state, Argentina
Szaibelyite (ascharite)	$Mg_2B_2O_5.H_2O$	41.4	China
Inderite	$Mg_2B_6O_{11}.15H_2O$	37.3	Kazakhstan
Kernite	$Na_2B_4O_7.4H_2O$	51.0	United-State
Datolite	$Ca_2B_2Si_2O_9.H_2O$	21.8	Russia

Boron deposits occur by evaporation and are almost always related with volcanic formations. The significant deposits are therefore restricted to three areas of the world: Turkey, South America and the USA. However, a further 73% of the world's sources of boron are located in Turkey. Most of these deposits, mined by open-pit mining methods, are found relatively close to the surface. These ores can be refined into pure chemical compounds.

The reserves of boron owning economical extent and superior concentration are found commonly in Turkey. It also found in dry high hydrothermal activity and volcanic zones of USA as compounds of the boron enclosed to oxygen. The greatest reserves of the boron are found in Turkey, United States, Russia, and South America (12).

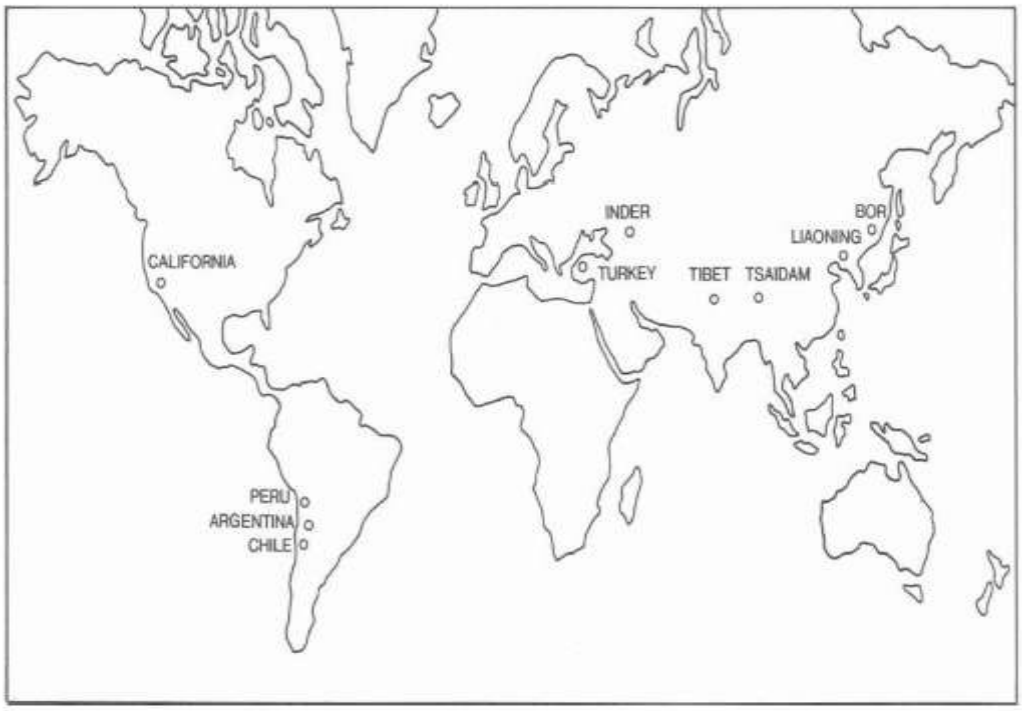

Figure 1.4. World Source of Boron Minerals

In the world, boron reserves known as boron deposits in Turkey contain 73%. It is known that there is a production capacity of around 5.7 million tons (2.7 million tons on B_2O_3 basis) in the world in 2017 (13). It is located in Bursa-Kestelek, Balıkesir Bigadiç, Eskişehir – Kırka and Kütahya-Emet. The conditions of reserves are Colemanite and Tinkal with the most plenty boron mineral in Turkey. Colemanite reserves are situated in Kütahya – Emet, Bursa – Kestelek and Balıkesir – Bigadiç. The Tinkal deposits are located in Eskişehir-Kırka in Turkey. More addition, the ulexite deposites can be found inthe Balıkesir-Bigadiç and are obtained as a by-product in Bursa- Kestelek (12). The reserve amounts of boron mineral in Turkey in Table 1.5.

Table 1.5. The reserves of boron the distribution in Turkey (2017 (13))

REGION	ORE TYPE	TOTAL(TON)
KESTELEK	Colemanite	5,254,920
BİGADİÇ	Colemanite-Ulexite	628,350,480
KIRKA	Tincal	824,720,950
EMET	Colemanite-Ulexite Probertite	1,811,072,520
	TOTAL	**3,269,398.87**

1.1.3. Usage Area of Boron

Boron products are applied in many areas such as in construction, nuclear energy, defense industry, chemistry, materials, agriculture, cleaning and healthcare. Concentrated boron products can also be consumed in these sectors, though regular boron products are used. Approximately 80% of boron products consumed global are concentrated in the detergent-cleaning sectors, ceramic, glass, and agriculture. Turkey is the leader country that performs the production of the refined boron products (14).

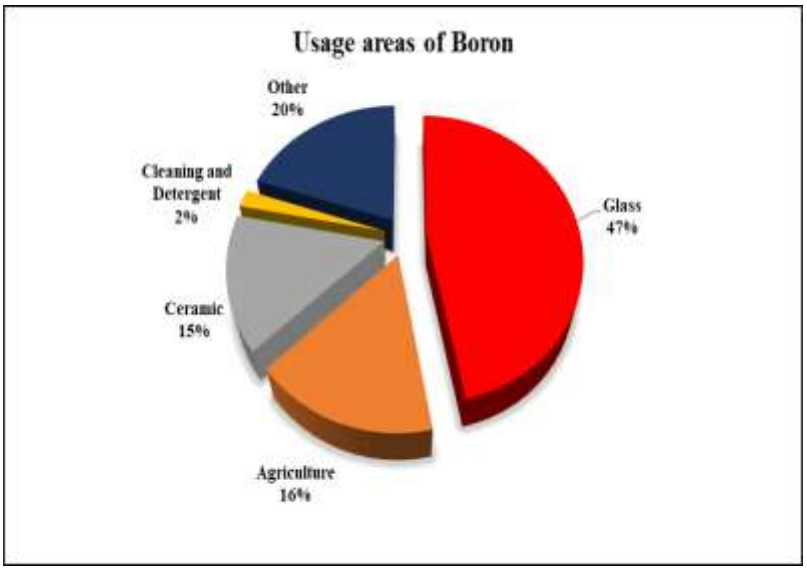

Figure 1.5. Usage Areas of Boron (15)

For thousands of years, boron also has been used in many scope implementation areas; energy, health, cement, agriculture, metallurgy, nuclear applications, glass, ceramic, flame retardant, boron fibers, cleaning and bleaching, aerospace (16).

1.2 BORATES and USES OF BORATES

Boron-containing borates, which can occur naturally in nature, are super materials developed for use in industry. When the naturally occurring borates are examined; Since boron contains hydrogen atoms, generally oxygen, metals, and a small amount of soil, water, and rock, which cannot be found in pure form in nature, they combine with other elements to compose borates and inorganic salts called boric acid (17).

Borates, which are known to be useful and harmless, are used in some chemistry fields with their super properties. Borates do not have a harmful effect on humans, nature or other living things when used under normal conditions for centuries. It is used as a bacteria, fungus and insect inhibitor in many applications from cosmetics to wooden structures. It is important for the development and formation of plants and is also used as a fertilizer ingredient in agriculture by increasing product quality and yield significantly. It is used as an adhesive in cosmetics and a viscosity in paints, with its ability to bind and hold together dispersed particles in different contents (18).

The most important compounds made by borates are borate fluorides, borate phosphates, and polyborates. The most important of the extraordinary physical properties of these compounds are light emission and non-linear optical properties.Its economic and unique chemical properties support the widespread use of borates. Detergents and bleaches, agricultural applications, glass fibers in textiles, glaze, fiberglass insulation, and enamel are the main areas of use (19).

Borates are formed by the bonding of elemental boron atoms and oxygen and contain B-O or B-OH groups in their structure. In simple borates, each boron atom is bonded to three oxygen atoms. For this reason, boron types such as H_3BO_3 contain only BO_3 units in their structures. The combined BO_3 units form various polymeric ring structures and chains. Besides BO_3 units, BO_4 units are also present in many complex borate structures (20).

The so-called basic building blocks of polymeric borate components contain

repeating and distinct polymeric subunits. This main building block is classified according to the coordination number of 3 or 4, as mentioned above, the boron in the repeating unit.

Borates are categorized in two ways, non-hydrated and hydrated borates. Hydrated borates contain H_2O crystalline water units and B-OH groups in their structure. Therefore, the basic borate units in the fully hydrated form are $B(OH)_3$ and $[B(OH)_4]^-$ The trigonal-BO_3 (Δ) group is formed by the bonding of the boron atom with the three-coordinated oxygen atom, and the tetragonal-BO_4 (T) group is formed as a result of the four-coordinated boron atom bonding with the oxygen.

Hexa Borates are borate types containing 3 BO_4 (T) and 3 BO_3 (Δ) groups in their structure. It is the OH groups and H_2O molecules that are coordinated with the metal cation in the system (21).

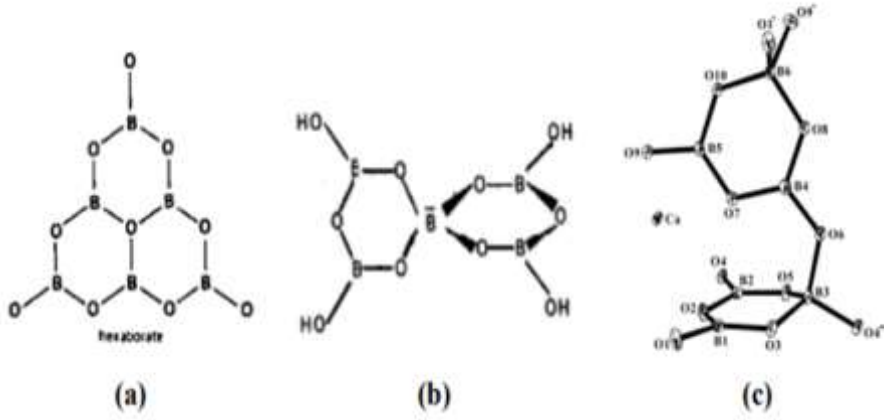

Figure 1.6. a) The position of the common oxygen atom in the ring and the BO3 groups in the hexaborate anion structure.**b)** The planar position of the BO4 groups is in the hexaborate anion structure.**c)** The hexaborate structure coordinated with the metal cation.

1.2.1. Classification and Structure of Borates

Minerals containing boron oxygen molecules or boric oxide are defined as borates. Various newly discovered borates of borate crystal contain BOn atomic groups. Borate compounds, which can be obtained mainly by the tetrahedral or trigonal coordination of the boron element, have been the subject of studies for most of the last century due to numerous structural types. Borates are categorized into three groups by Carpeni: pentaborates, tetraborates, and orthoborates or metaborates in the given Figure 1.7 The categorization was made according to the basicity and the number of boron atoms of the anion (22).

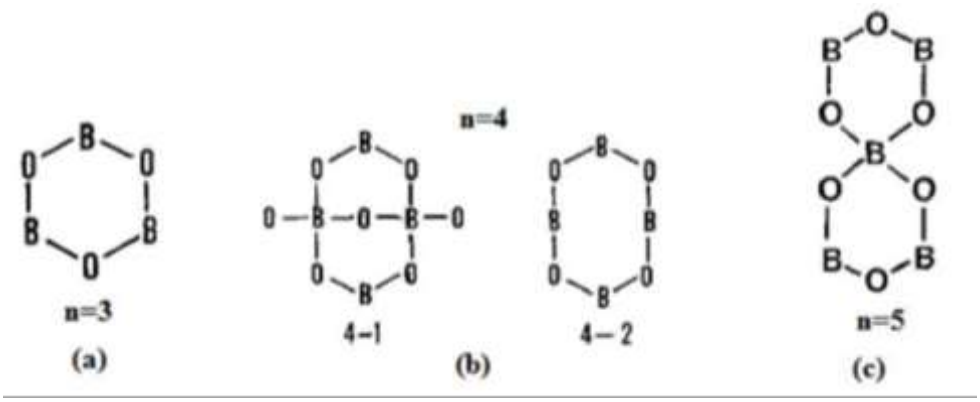

Figure 1.7. Structure of a) metaborate, b) tetraborate, c) pentaborate

Possible bonding types of boron to form borate polyanions are given in Figure 1.8.

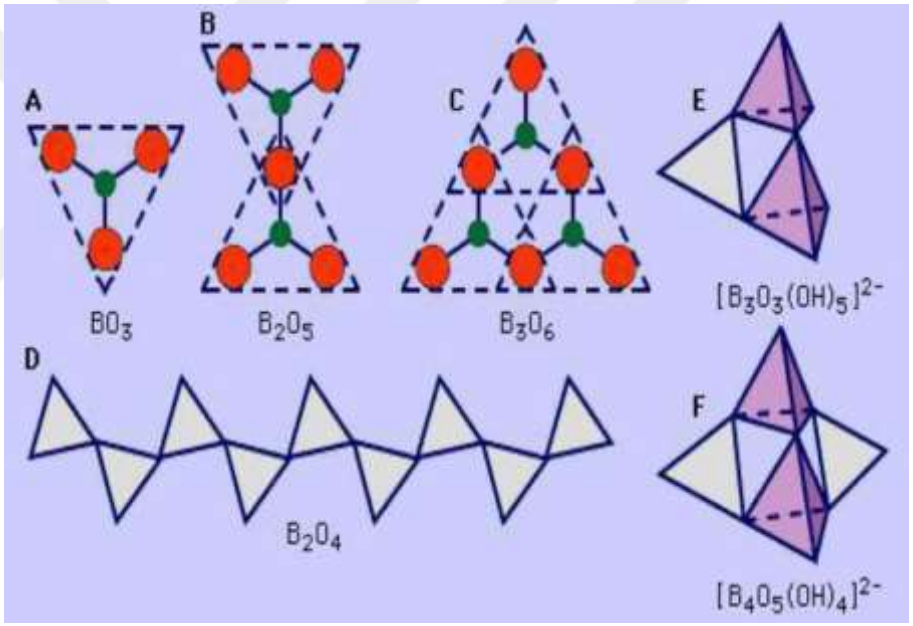

Figure 1.8. Boron bonding patterns (A) BO_3 trihedral, (B,C) multiple groups, (D) borate chains, (E) trihedral and (F) tetrahedral group complexes

1.2.2. Metal Borates

Oxygen-only metal borates, both in artificial and mineral forms, are numerous and many of them are widely used in industry. Artificial metal borates are structurally similar to minerals containing complex multiborate rings or separated multiborate ions, layers, chains, or networks (17). The basic structural principles of bonds in crystal metal borates are as follows:

1. In aqueous borates, protons first convert free O^{-2} ions to free OH^- ions.

2. The remaining protons are used by the oxygens in the trihedral and tetrahedral planes in the borate ion. The added protons then convert the free OH^- ions into the water.

3. It can be exchanged with multiple anions of the complex borate with the addition of a single edge group.

4. The others that may exist in the existence of anions are isolated $B(OH)_3$ groups, or their polymers (17).

1.2.3. Zinc Borate

Zinc borate is used in many industries such as ceramics, cables, cement, electrical insulation, rubber, pharmaceuticals, wood applications, paint, and plastic, according to its properties. Zinc borates are generally used as flame retardant in nylons and halogenated polyesters, in electrical/electronic parts, fabrics, automobile/aircraft interiors, as smoke suppressant and corrosion retardant, in PVC, ceramics industry as a melting point reducer (Flux) and as boron silicate glass raw material. Zinc borates are commonly applied as a flame retardant in rubber and plastic products (27).

It helps to decrease the loss of life and feature to minimal levels, in this way provides period for the initial intervention to fire in the event of possible fires. Zinc Borate, manufactured with boron products and boron that do not menaced human health, supply long-lasting usage in application areas compared and a more durable to chemical products (28).

Zinc borate has wide commercial use and is a colorless, non-hygroscopic, white, powdery substance. High dehydration temperature and low solubility in water are the most important features of zinc borate. $2ZnO.3B_2O_3.3,5H_2O$ and $2ZnO.3B_2O_3.3H_2O$, which are widely used with high dehydration temperature called anhydrous zinc borate, can reach high temperatures, but can hydrolyze with strong acids and bases. With this feature, the water molecules in the composite are removed before reaching the ignition temperature, and it provides resistance to fire by covering the surface of the coal formed and preventing further combustion (23).

Zinc borate, whose mole ratio of ZnO/B_2O_3 is determined, is the determining factor in its structure and properties in different crystal types. This ratio varies between 0.25 and 5.

Zinc borates, which are in the inorganic hydrate borate group, can also be classified into synthetic hydrate borates. The chemical composition of zinc borates can be shown as $xZnO.yB_2O_3.zH_2O$.

The structure of molecular zinc borate is presented in Figure 1.9.

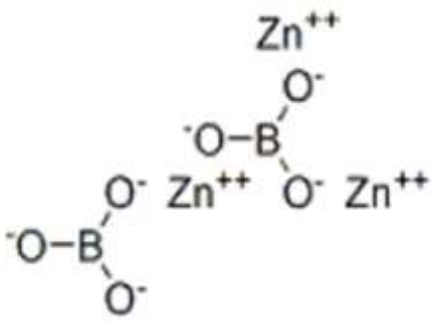

Figure 1.9. Molecular structure of zinc borate

There are many different Zinc borates, depending on the amount of water they contain and the zinc/borate ratios in their formula. The most well-known of these is the compound $2ZnO.3B_2O_3.3.5H_2O$. Other known Zinc borates:

$2ZnO.3B_2O_3.7H_2O$,

$ZnO.B_2O_3.2H_2O$,

$2ZnO.3B_2O_3.3.5H_2O$,

$ZnO.B_2O_3.H_2O$,

$6ZnO.5B_2O_3.3H_2O$

$ZnO.5B_2O_3.4.5H_2O$,

$4ZnO.B_2O_3.H_2O$,

$3ZnO.5B_2O_3.14H_2O$,

$4ZnO.B_2O_3.H_2O$,

$2ZnO.2B_2O_3.3H_2O$,

$2ZnO.3B_2O_3$

In recent years borates have important practical applications and have attracted great interest, it is known that the most common used zinc borate is $2ZnO.3B_2O_3.3.5H_2O$ compound, and it was determined that the molecular formula of this compound is $2ZnO{\cdot}3B_2O_3{\cdot}3H_2O$ (24-25). Zinc-containing borates have been investigated because of their potential value as optical and catalysis materials. At least three ends of $ZnO–B_2O_3$ have been proposed, including the binary group,

$Zn_4O(BO_2)_6$, ZnB_4O_7 and $Zn_3B_2O_6$. The crystal structure of $Zn_3B_2O_6$ is given in Fig 1.10 (26).

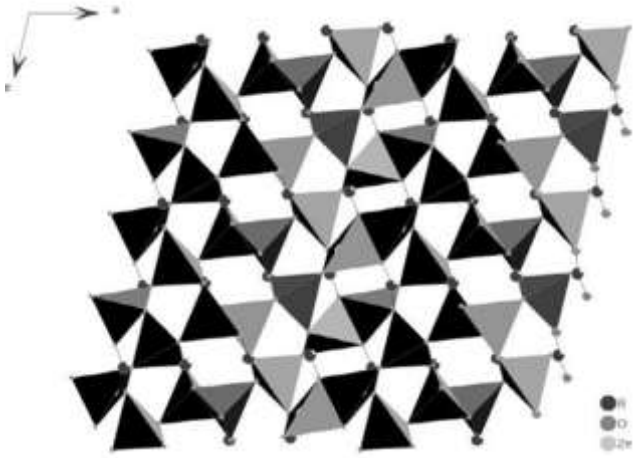

Figure 1.10. Crystal structure of $Zn_3B_2O_6$

BO_3 triangles have several orientations in both α and β-$Zn_3B_2O_6$ and ZnO_4 tetrahedra have diverse connection modes.

In α-$Zn_3B_2O_6$, every ZnO_4 tetrahedron is connected to the four others by the same corners to form three dimensional Zn–O frameworks. To enhance the structure of zinc orthoborates, the boron atoms in the structures are linked to the triangular hollows of oxygen in the networks. The six ZnO_4 tetrahedra are corner-sharing to each BO_3 triangles while BO_3 triangles are seperated from each other, as shown in Fig 1.11 and 1.12 (26).

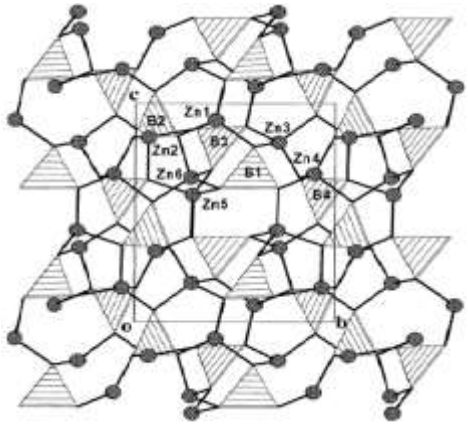

Figure 1.11. The crystal structure of α-$Zn_3B_2O_6$ projected along the [1 0 0] direction

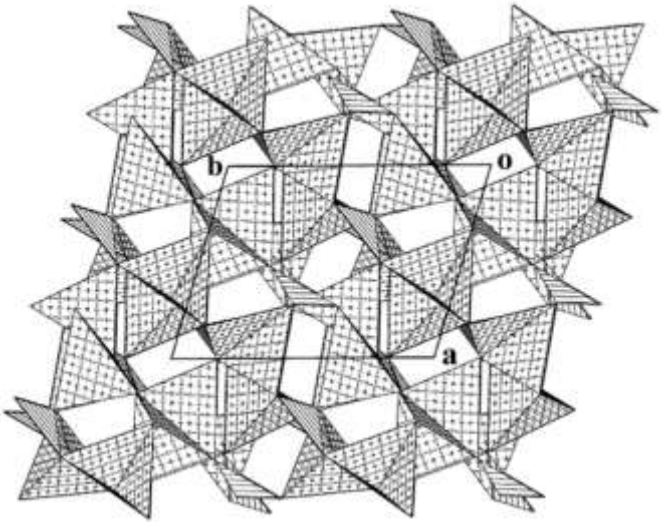

Figure 1.12. The crystal structure of α-$Zn_3B_2O_6$ projected along the [0 0 1] direction.

In the β-$Zn_3B_2O_6$, the crystal structure are also consists ZnO_4 tetrahedra and BO_3 triangles that connected to eah other by corner-sharing in Figure 1.13. (26).

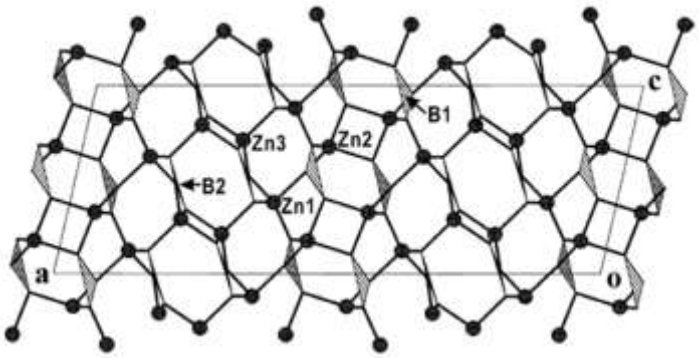

Figure 1.13. View of the β-$Zn_3B_2O_6$ structure along the *b*-axis.

The characteristics of alpha and beta form of zinc orthoborates have been studied by Chen et al. The high temperature, β-$Zn_3B_2O_6$ and low temperature, α-$Zn_3B_2O_6$ borates have been prepared with solid-state method. It was reported by Chen et al. that the α-$Zn_3B_2O_6$ and β-$Zn_3B_2O_6$ crystallizes in a triclinic space group $P^{-}1$ and in a monoclinic group *C*2/*c*, respectively (26).

In 2005, D.-G. Chen et al has used H_3BO_3, ZnO and V_2O_5 as starting materials for the preparation of zinc vanadoborate. During the preparation process the crystal of $Zn_3B_2O_6$ are obtained unexpectedly. It is possible that the V_2O_5 carried as a flux in the crystal growth of $Zn_3B_2O_6$. Various experiments have been done by high temperature solution reaction. The monoclinic phase of zinc

orthoborate was successfully obtained (29).

α-$Zn_3B_2O_6$ precipitated transparent glass ceramics have produced by Hirokazu M et al. The precipitated α-$Zn_3B_2O_6$ was analyzed by TEM and XRD techniques. The effect od CaO and Al_2O_3 are effected the crystallized form of precipitated α-$Zn_3B_2O_6$ during the preparation process (30).

Xin-Guang W et al. has successfully prepared $Zn_3B_2O_6$ by the solid-state reaction method using ZnO and H_3BO_3 starting materials have been synthesized zinc borate with low annealing temperature. The ranges of heating temperatures are from 875°C to 950°C. It is stated that best results of dielectric properties was obtained at 925°C (31).

In last few years, the luminescences studies of rare earth metal doped $Zn_3B_2O_6$ have been done by many scientists due to its high quantum efficiency in the visible region. The $Zn_3B_2O_6$ are defined in monoclinic form where the triangles of BO_3 are edge-sharing with the tetrahedral of ZnO_4. The $Zn_3B_2O_6$ compounds are innately demonstrate the unique optical properties such as thermoluminescence and luminescent behavior because of the existence of ZnO_4 clusters. These properties made the $Zn_3B_2O_6$ can be carried out in grand scale of applications.

G.V.S.S. Sarma et al has been synthesized the Mn^{2+} doped $Zn_3B_2O_6$ nanopowder by co-precipitation method. The resulted powder samples are characterized SEM with EDS, XRD and other characteristic methods (32).

The preparation of red emitting β-$Zn_3B_2O_6$:Mn^{2+} has also been synthsized by a solid-state reaction technique. Mn^{2+} doped β-$Zn_3B_2O_6$ crystal structure has been examined cathodoluminescent and photoluminescent properties. The results verify that β-$Zn_3B_2O_6$:Mn^{2+} matches the UV LED chip (33).

Co-precipitation method has been used in the synthesis of Co^{2+} and Ni^{2+} doped $Zn_3B_2O_6$ nano crystalline powders. The $Zn(NO_3)_2.6H_2O$ and $Na_2B_4O_7.10H_2O$ as starting materials. The characterization process has carried out by SEM with EDS, UV/VIS absorption, XRD, FT-IR and photoluminescence spectroscopies methods. Results of analysis show that the products have monoclinic structure (34).

Reddy et al. has been reported preparation of $Zn_3B_2O_6$ doped copper ions using co-precipitation method with starting materials of $Zn(NO_3)_2.6H_2O$ and $Na_2B_4O_7.10H_2O$. The crystal structure, energy level structure, the nature of site symmetry, lattice distortion, luminescent properties and bonding nature in order to

the synthesized products have been studied using different spectroscopic techniques. The X-ray diffraction, optical and EPR studies has been applied to characterize the obtained products. It is showed that products are in monoclinic crystal structure and sistorted in octahedral site symmetry (35).

Ce^{3+} and Al^{3+} doped zinc orthoborate nanoparticles were synthesized by co-precipitation method and the effect of Al^{3+} on luminescence properties of Ce^{3+} was determined(Zou et al). In 2017, sol-gel method has been also carried out in the preparation of doped β-$Zn_3B_2O_6$ applying zinc nitrate and boric acid as starting agents. It is determined that the transformation of gel into single phase β-$Zn_3B_2O_6$ at 700^{o}C (3hours) annealing temperature. The characterization of as-prepared products have been examined using FT-IR, DRS, EDS, XRD and SEM. Furthermore, the effect of acid type, gelling agent, acid:gelling agent ratio on the morphology and the size of structures were also determined (36).

Using ZnO, H_3BO_3, Eu_2O_3 and Li_2CO_3 as starting materials, the pure co-doped $Zn_3B_2O_6$ with Eu^{3+} and Li^+ ion by solid state reaction has synthesized by Zhou et al (2018). The calcination process was done at 800^{o}C for 2 hours and the structural properties of the obtained products were done by XRD techniques. It is reported that the products were characterized in monoclinic phase and the lattice constants are a =23.43, b=5.046 and c=8.385 (37).

Kui et al have investigated the Low temperature co-fired ceramic (LTCC) which widely used in the multi-layer technology for the electronic devices packages and circuit. The studies were done based on its dielectric properties, sintering temperature and microstructure. Zinc borate can effectively provide a liquid sintering help for the low-temperature fabrication of the composite ceramics (38).

Li doped $Zn_3B_2O_6$ were also prepared by solid-state reaction method using ZnO, H_3BO_3 and Li_2CO_3 and the characterization studies were done by X-ray diffraction, Raman spectroscopy, microwave dielectric properties, FT-IR, SEM and EDS. The analysis result showed that $Zn_3B_2O_6$ has monoclinic structure andobtained at sintering temperature of 850^{o}C for 3 hours. It also reported that the electric polarization and phase structure stability were affected by the bond ionicity and lattice energy of the B–O bond of the obtained products (39).

The substitution of Mn^{2+} to $Zn_3B_2O_6$ ceramic was synthesized through solid state reaction method with including ZnO, MnO and B_2O_3 as raw materials. The characterization of resulted has been examined TG, DSC, TMA, XRD, SEM. The

substitution process was accomplished as Zn site has lowest energy and allow the Mn^{2+} to occupy in the $Zn_3B_2O_6$ crystal. The ion-substitution of Mn^{2+} into the tetrahedron of ZnO_4 resulting in the replacement of electron distribution and the bond property (40).

Using ZnO and H_3BO_3 as raw powders have been synthesized via the conventional solid-state reaction method. The as synthesized products have been examined using, densification process analysis SEM and XRD. The microwave dielectric properties were also determined. In the XRD and SEM analysis the crystal structure (monoclinic) and the size distribution were observed, respectively. It is also stated that the optimization of the dielectric properties was able to obtained by varying annealing temperatures (41).

1.3 SYNTHESIS METHOD OF BORATES

Owing to its promising applications and properties, borates have attracted many considerations attentions as different methods have been improved for the preparation of zinc borate materials. Different synthesis methods have been improved to prepare high-grade borate compounds, like hydrothermal, sonochemical method, co-precipitation method, solid-state method, microwave method, sol-gel method, solution combustion synthesis, etc.

Zinc borate is generally obtained as a result of boric acid and zinc oxide reaction as raw materials at a stoichiometric ratio. The boric acid used should be around 5% to 10% for all of the zinc oxides in the environment to turn into a product (26).

1.3.1. Solution Combustion Synthesis (SCS) Method

Solution methods have been widely applied as synthesis method due to their impressive typical which elevated the purity dust with small particle size. The solution combustion method, known as combustion synthesis, was first carried out as by Merzhano et al in 1967. Due to its large particle size and difficult accessibility, it was combined with a wet chemistry and upgraded to solution combustion synthesis by Patil et al.

Solution combustion synthesis (SCS) is a variable process which admitted much attention on account of its talent to synthesize nanosized products in controlled sized and composition depending on the exothermicity of the reduction-oxidation reaction. Metal salts like sulfates, nitrates, and carbonates as oxidizing

agents (oxidant), and starch, sucrose, urea, glycine etc. as reducing agent are used in solution combustion synthesis.

The mechanism of reaction with the solution combustion process is based on a great deal variants like the amount of water, fuels, fuel-oxidizer, oxidizer used during starting ingredients and the ignited temperature between 300-500°C. Since the amount of fuel can affect the physical properties and crystallinity of the product, it take part a very substantial role. The compound consider as the best fuels and oxidizers if they have high solubility level in the solvent, readily present, low-priced and has low decomposition temperature (42).

2. AIM AND SCOPE OF THE STUDY

The first aim of this study is to synthesize zinc orthoborates formulated as $Zn_3B_2O_6$ by economical yet simpler process; solution combustion synthesis method. The term of reaction are diverse by differing the organic fuels such as urea, glycine, tartaric acid, HMTA, citric acid, and β-Alanine. Furthermore, the heating temperature are also varied to investigate their impact on the crystal structure, crystallite sizes and optical properties.

Secondly, The crystal structure of synthesized borates as triclinic alpha and monoclinic beta forms of zinc orthoborates will be characterized by XRD technique. In addition, to predict the nanosized particle of the products obtained the crystallite sizes will be calculated by Debye-Scherrer's equation.

Thirdly, the vibrational motions of B-O bond in triangle BO_3 group in orthoborates will be assigned via FTIR spectroscopy method.

In the last part of this thesis, the optical properties will be investigated considering the absorbance and reflectance spectra taken by UV-VIS and DRS studies.

3. MATERIALS AND METHODS

3.1 CHEMICALS

In this work, the chemicals that were used are presented as follows;

$Zn(NO_3)_2.6H_2O$, Zinc nitrate hexahydrate: Merck (pure 99.0%)

H_3BO_3, Boric acid: Merck, 99.00%

CH_4N_2O , Urea : Merck, 99.50%

$C_2H_5NO_2$, Glycine : Merck, 99.70%

$C_4H_6O_6$, Tartaric acid : Merck, 99.00%

$C_6H_{12}N_4$, Hexamethylenetetramine (HMTA) : 99.90%

$C_6H_8O_7.H_2O$, Citric acid monohydrate : Merck, 99.50%

$C_3H_7NO_2$, β-Alanine: Merck (pure 99.0%)

KBr, Potassium Bromide , for IR Spectroscopy : Merck, 99.90%
It was dried for 2 hours at 180^oC before using.

3.2 INSTRUMENTS

3.2.1 X-ray Powder Diffractometer

Figure.3.1. The image of X-ray Powder Diffractometer (XRD)

To examined the structural properties of the obtained compound, the Rigakuminiflex and multiflex X-ray powder diffractometer with CuKα (30-40kV, 1020mA, λ=1,54056 Å) radiation were used and the obtained data were compared with the ICDD data card.

3.2.2 Fourier Transform Infrared Spectrophotometer

Figure 3.2. The image of Fourier Transform Infrared Spectrophotometer.

The Perkin Elmer Fourier Transform Infrared (FTIR) spectrophotometer in the region of 4000-400 cm^{-1} was operated to determine the infrared spectra and bond variation of the final products. Thw Infrared spectra was recorded by preparing the pellets that are prepared by 0.1500:0.0010 (wt/wt) of KBr:product ratio.

3.2.3 UV- VIS Spectrometer

Figure.3.3. The image of UV-VIS Spectrophotometer.

Perkin Elmer Lambda 35 UV-VIS Spectroscopy at range of wavelength 200-900 nm was applied to record to ascertain the optical properties of the products. The obtained spectra were plotted by using Data Processor WinLab program.

3.2.4 Furnace

Figure.3.4. The image of furnace.

The reactions during the preparation of metal borates and the annealing process were done by using Nuve MF 120 furnace in the range of 400-900^{o}C.

3.3 METHODS

The preparation of zinc orthoborates were successfully done by Solution Combustion Synthesis (SCS) method. The starting materials are zinc nitrate hexahydrate $Zn(NO_3)_2.6H_2O$, H_3BO_3 and different kinds of fuels such as beta-alanine, citric acid, glycine, HMTA, tartaric acid and urea. For the source of Zn and B, $Zn(NO_3)_2.6H_2O$ and H_3BO_3 were applied, respectively.

3.3.1 Synthesis of Zinc Orthoborate

Zinc orthoborates were prepared by using solution combustion synthesis methos. For this purpose, the stoichiometric amounts of $Zn(NO_3)_2.6H_2O$, H_3BO_3, and fuels were mixed and dissolved in minimum amount of distilled water. The homogeneous mixture was stirred continuously on a magnetic stirrer until a gel-like residue was observed at 370°C and allowed to evaporate. The gel residue was introduced to the preheated furnace for 10 minutes at 400°C. It is observed that different colors of the as-prepared product were obtained depending on the applied fuels. The annealing process was completed at different temperatures for one hour at the range of 400°C-900°C. The characterization of the obtained products were studied and compared.

Figure 3.5. The image of experimental procedure part of synthesis

Similar process written above was carried out by using various fuels and the expected reactions are presented as follows;

Urea

$3Zn(NO_3)_2.6H_2O(s) + 2H_3BO_3(s) + 5CH_4N_2O(s) \rightarrow Zn_3B_2O_6(s) + 8N_2(g) + 5CO_2(g) + 31H_2O(g)$

Glycine

$18Zn(NO_3)_2.6H_2O(s) + 12H_3BO_3(s) + 20C_2H_5NO_2(s) \rightarrow 6Zn_3B_2O_6(s) + 28N_2(g) + 40CO_2(g) + 176H_2O(g)$

Tartaric Acid

$3Zn(NO_3)_2.6H_2O(s) + 2H_3BO_3(s) + 3C4H6O6\ (s) \rightarrow Zn_3B_2O_6(s) + 3N_2(g) + 12CO_2(g) + 30H_2O(g)$

HMTA

$18Zn(NO_3)_2.6H_2O(s) + 12H3BO3(s) + 5C6H12N4(s) \rightarrow 6Zn_3B_2O_6\ (s) + 28N2(g) + 30CO2(g) + 156H2O(g)$

Citric Acid

$18Zn(NO_3)_2.6H_2O(s) + 12H3BO3(s) + 10C6H10O8(s) \rightarrow 6Zn_3B_2O_6\ (s) + 18N2(g) + 60CO2(g) + 176H2O(g)$

β-Alanine

$3Zn(NO_3)_2.6H_2O(s) + 2H_3BO_3(s) + 2C3H7NO2\ (s) \rightarrow Zn_3B_2O_6(s) + 4N_2(g) + 6CO_2(g) + 28H_2O(g)$

4. RESULTS AND DISCUSSION

4.1 The Solution Combustion Synthesis of Zinc Orthoborate

The Solution Combustion Synthesis (SCS) were applied in the synthesis of the zinc orthoborate by tuning the fuels and heating temperatures. The applied fuels are beta-alanine, citric acid, glycine, HMTA, tartaric acid and urea. In more addition, the heating process were done in the range of 400-900^{o}C for an hour.

Dissimilar attitude of the solution was observed throughout the preparation of $Zn_3B_2O_6$. The fuels evolved more gases in the synthesis, manufacture different colors and also different tissue of powder after the preheated process.

The fuels used in SCS are individually described below.

Urea:

The homogeneous solution was blurry and formed a colorless gel at 370°C. The proportion of evolved gas was normal. After preheating for 10 minutes at 400°C, a white hard product was occurred.

Picture 4.1 The images of $Zn_3B_2O_6$ samples for urea fuel a) gel form, b) synthesis

Glycine:

The colorless gel was observed at 370°C and produced a little proportion of gas evolved. After preheating for 10 minutes at 400°C, a fluffy light brown product was obtained.

a b

Picture 4.2 The images of $Zn_3B_2O_6$ samples for glycine fuel a) gel form, b) synthesis

Tartaric Acid:

The colorless homogeneous solution was turned into yellow-like gel after continuously stirred at 370°C. The amount of gas evaporated was normal. After preheating for 10 minutes at 400°C, a brown fluffy soft product was obtained.

a b

Picture 4.3 The images of $Zn_3B_2O_6$ samples for tartaric acid fuel a) gel form, b) synthesis

HMTA:

After dissolving the starting materials in small amount of distilled water, the homogenized solution was colorless and produced a cloudy white gel at 370°C. The proportion of gas that evolved was normal. After preheating for 10 minutes at 400°C.A yellowish-white product was a little harsh and hardly to stored from evaporating dish.

a b

Picture 4.4 The images of $Zn_3B_2O_6$ samples for HMTA fuel a) gel form, b) synthesis

Citric Acid:

The homogeneous solution was uncolored and created a yellowish precursor-gel at 370°C. The evaporation of gas was high and when precursor-gel started to form it evolved yellow gas. After preheating for 10 minutes at 400°C.A light cream fluffy produce was obtained.

a b

Picture 4.5 The images of $Zn_3B_2O_6$ samples for CA fuel a) gel form, b) synthesis

β-Alanine:

The homogeneous solution was colorless gel at 370°C and produced a little proportion of gas evolved. After preheating for 10 minutes at 400°C.The precursor gel was colorless. The fluffy brown as-prepared product was stuck on the evaporating dish and a bit harsh.

Picture 4.6: The images of $Zn_3B_2O_6$ samples for B-AL fuel a) gel form, b) synthesis

4.1.1 Structural Characterization Studies of Zinc Orthoborate

The structural properties of zinc orthoborate were determined by taking the as-synthesized product obtained at 400^{o}C 10 minutes and heated at higher temperatures between 400^{o}C to 900^{o}C. The characterization processes were done by X-Ray Diffraction to examine the crystallite size and crystal structures, FT-IR to identify vibrational modes.

4.1.1.1. FT-IR Spectroscopy Studies

The infrared spectra of zinc orthoborate are given in figures 4.1-4.7. The strong and broad band at about 2800-3600 showed the –OH group stretching vibration of water molecules. In the FTIR analysis of borates, the modes vibrations of borate mesh have three areas and the vibration bands are intensively detected at the range of 2000–500 cm^{-1}.

In the FTIR spectrum, BO_3 group is triangular, the vibrations are in the area of ν_3 = 1100–1400 cm^{-1} which assigned to B–O asymmetric stretch, the band

at ν_2 = 700–900 cm^{-1} is contributed to out-of-plane bend, whereas the one at ν_1 = 900–1000 cm^{-1} belongs to the B–O symmetric stretch. The band at around 600 cm^{-1} is appointed to stretching vibration of Zn–O. The BO_3 groups are the fundamental structural units in the zinc orthoborate crystal structure (26).

It observed that zinc orthoborates were produced by various fuels. In FT-IR analysis, it is showed that there is no significant difference observed in the FT-IR spectra (Table 4.1-4.7).

Table 4.1. FTIR Assignment of $Zn_3B_2O_6$ with all fuels and wavenumbers (cm^{-1}) at 400°C

$Zn_3B_2O_6$	**BO_3 Asymmetric Stretching (cm^{-1})**	**BO_3Symmetric Stretching (cm^{-1})**	**BO_3Bending (cm^{-1})**
ß-Alanine	1221.49	1065.97	716.12
Citric Acid	1228.24	1015.45	718.80
Glycine	1243.20	1012.93	711.88
Hmta	1243.05	1050.93	717.99
Tartaric Acid	1234.53	1015.18	703.19
Urea	1241.31	1013.65	708.94

Table 4.2. FTIR Assignment of $Zn_3B_2O_6$ with all fuels and wavenumbers (cm^{-1}) at 500°C

$Zn_3B_2O_6$	**BO_3 Asymmetric Stretching (cm^{-1})**	**BO_3Symmetric Stretching (cm^{-1})**	**BO_3Bending (cm^{-1})**
ß-Alanine	1221.77	1065.91	716.47
Citric Acid	1227.60	1017.35	720.20
Glycine	1243.20	1013.43	713.87
Hmta	1230.81	1065.88	718.39
Tartaric Acid	1231.68	1014.95	703.04
Urea	1220.34	1014.85	696.83

Table 4.3. FTIR Assignment of $Zn_3B_2O_6$ with all fuels and wavenumbers (cm^{-1}) at 600°C

$Zn_3B_2O_6$	**BO_3 Asymmetric Stretching (cm^{-1})**	**BO_3Symmetric Stretching (cm^{-1})**	**BO_3Bending (cm^{-1})**
ß-Alanine	1244.88	933.77	720.10
Citric Acid	1243.79	933.73	719.50
Glycine	1239.28	933.73	719.90
Hmta	1244.07	933.73	719.48
Tartaric Acid	1244.36	933.74	718.89
Urea	1228.60	933.74	718.97

Table 4.4. FTIR Assignment of $Zn_3B_2O_6$ with all fuels and wavenumbers(cm^{-1}) at 700°C

$Zn_3B_2O_6$	**BO_3 Asymmetric Stretching (cm^{-1})**	**BO_3Symmetric Stretching (cm^{-1})**	**BO_3Bending (cm^{-1})**
ß-Alanine	1227.10	971.34	719.34
Citric Acid	1235.42	971.34	718.43
Glycine	1235.71	971.34	718.99
Hmta	1237.84	971.55	720.10
Tartaric Acid	1237.61	971.55	717.65
Urea	1234.83	971.45	718.35

Table 4.5. FTIR Assignment of $Zn_3B_2O_6$ with all fuels and wavenumbers(cm^{-1}) at 800°C

$Zn_3B_2O_6$	**BO_3 Asymmetric Stretching (cm^{-1})**	**BO_3Symmetric Stretching (cm^{-1})**	**BO_3Bending (cm^{-1})**
ß-Alanine	1236.57	971.47	718.24
Citric Acid	1235.95	971.49	719.36
Glycine	1239.06	971.47	722.05
Hmta	1237.13	971.23	719.98
Tartaric Acid	1237.57	971.87	717.91
Urea	1235.89	971.87	715.54

Table 4.6. FTIR Assignment of $Zn_3B_2O_6$ with all fuels and wavenumbers (cm^{-1}) at 900°C

$Zn_3B_2O_6$	**BO_3 Asymmetric Stretching (cm^{-1})**	**BO_3 Symmetric Stretching (cm^{-1})**	**BO_3Bending (cm^{-1})**
ß-Alanine	1236.14	971.01	718.25
Citric Acid	1235.01	971.34	718.39
Glycine	1234.23	971.20	717.80
Hmta	1236.20	970.54	718.15
Tartaric Acid	1236.39	971.12	718.97
Urea	1236.39	971.20	716.27

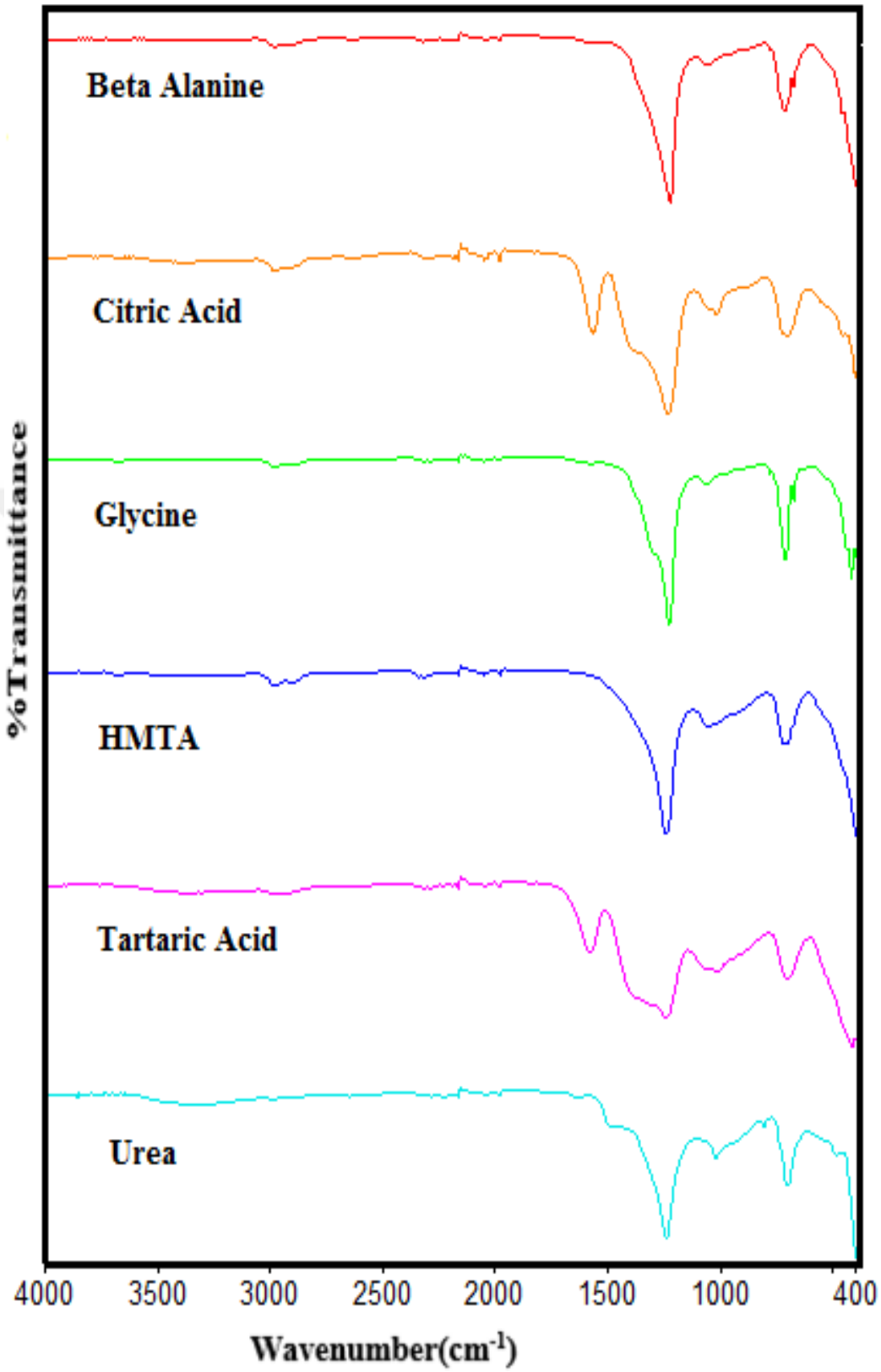

Figure 4.1. FT-IR Spectra of Synthesis $Zn_3B_2O_6$ Using All Fuels

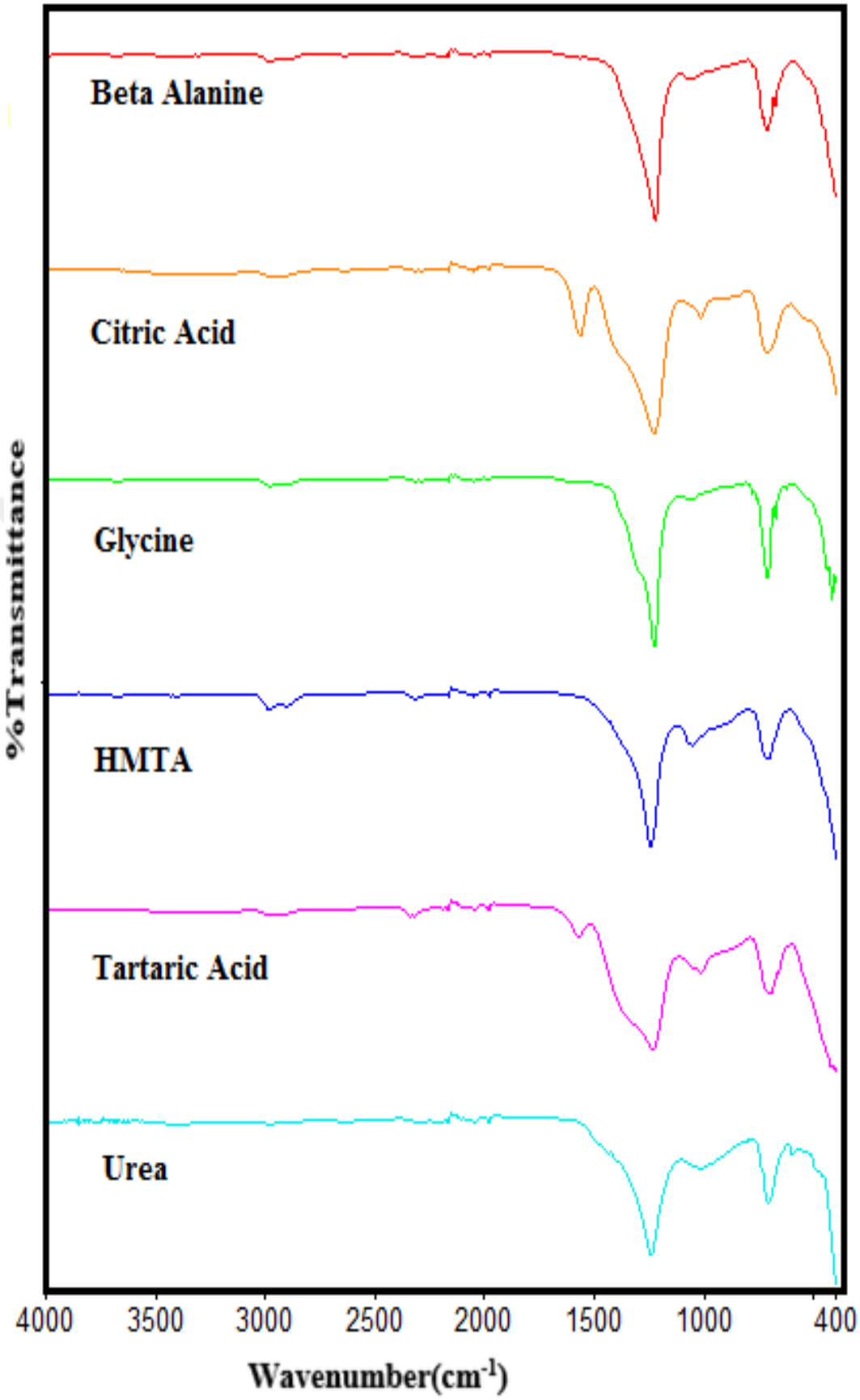

Figure 4.2. FT-IR Spectra of $Zn_3B_2O_6$ at 400°C Using All Fuels

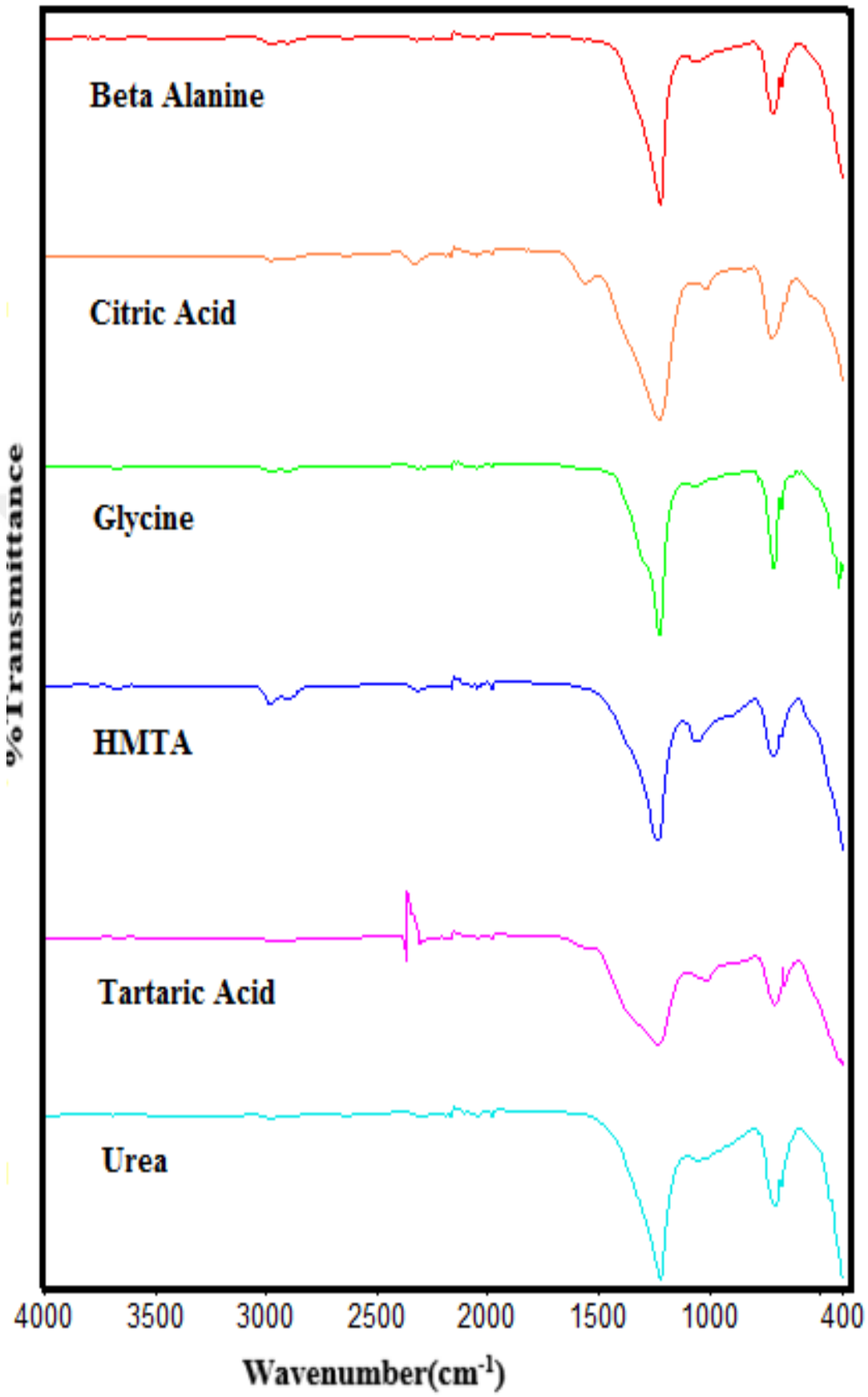

Figure 4.3. FT-IR Spectra of $Zn_3B_2O_6$ at 500°C Using All Fuels

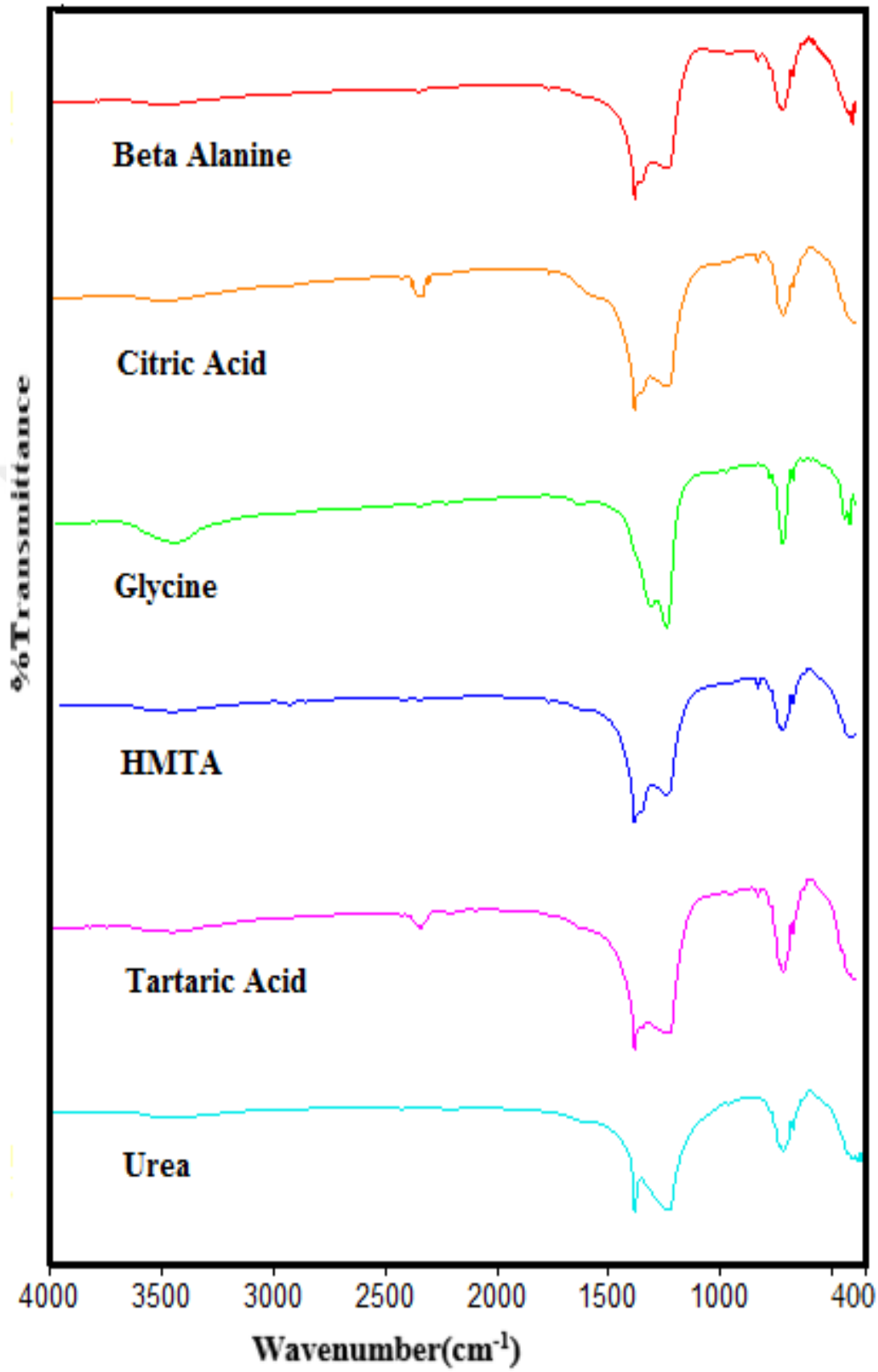

Figure 4.4. FT-IR Spectra of $Zn_3B_2O_6$ at 600°C Using All Fuels

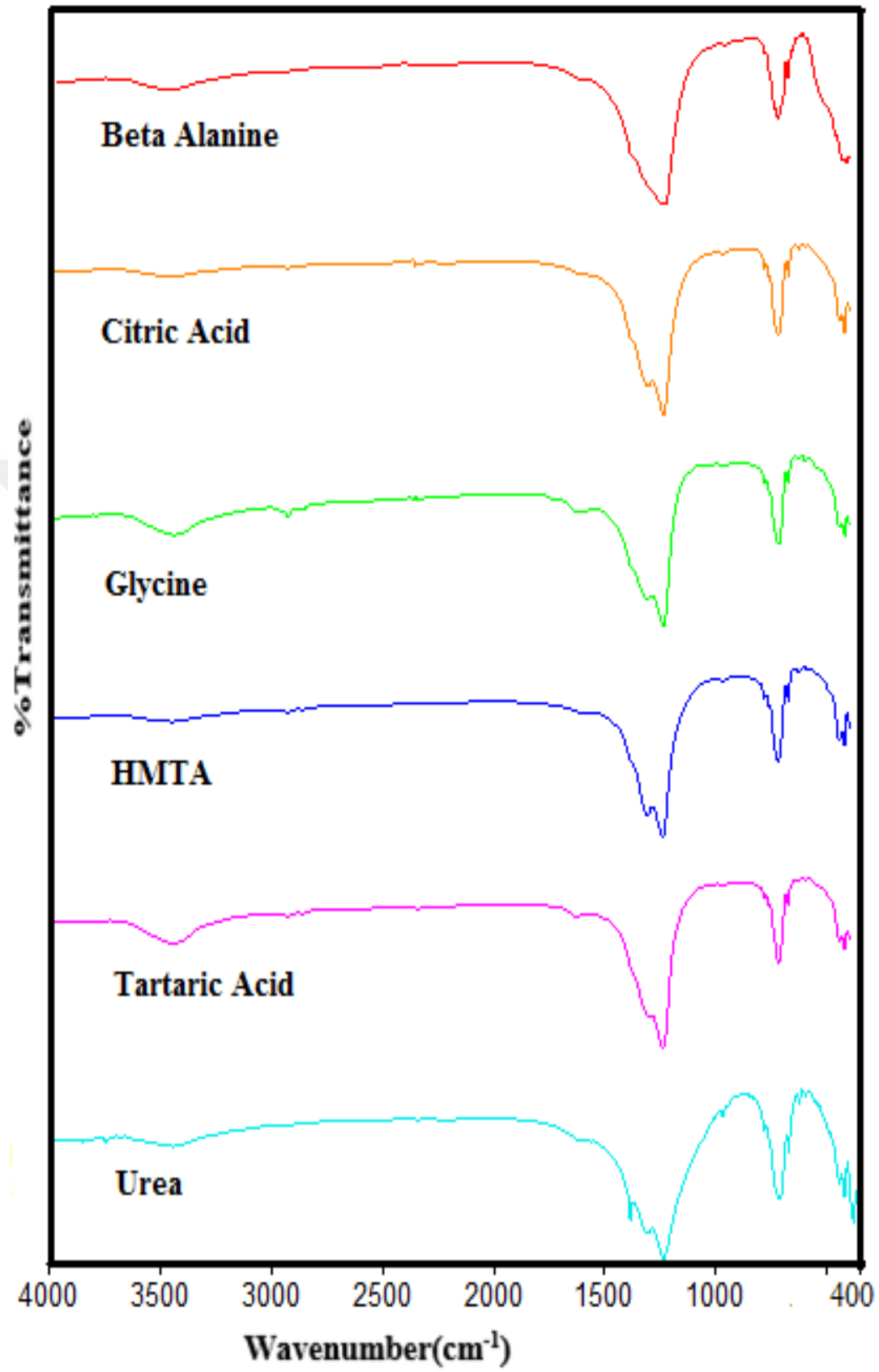

Figure 4.5. FT-IR Spectra of $Zn_3B_2O_6$ at 700°C Using All Fuels

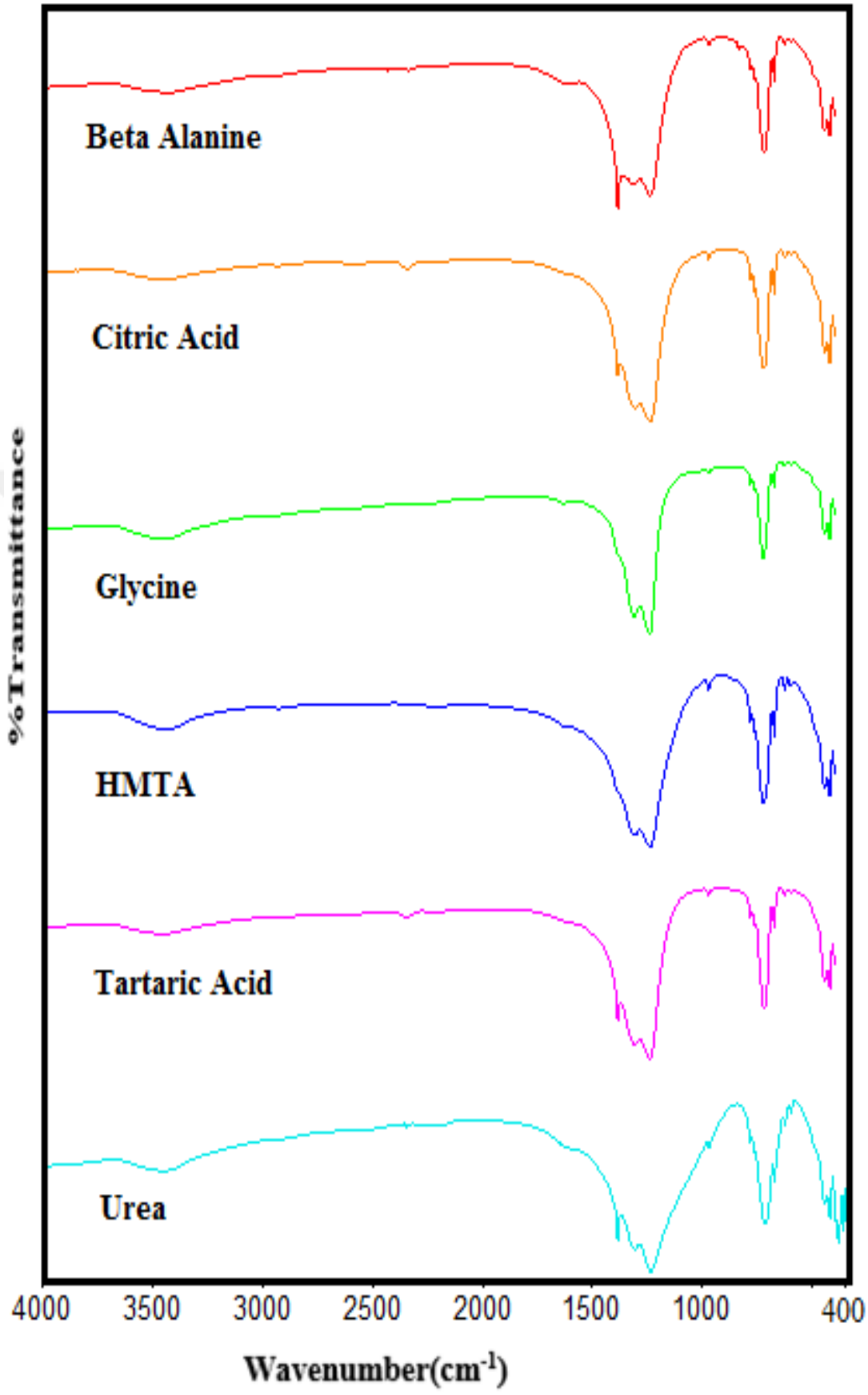

Figure 4.6. FT-IR Spectra of $Zn_3B_2O_6$ at 800°C Using All Fuels

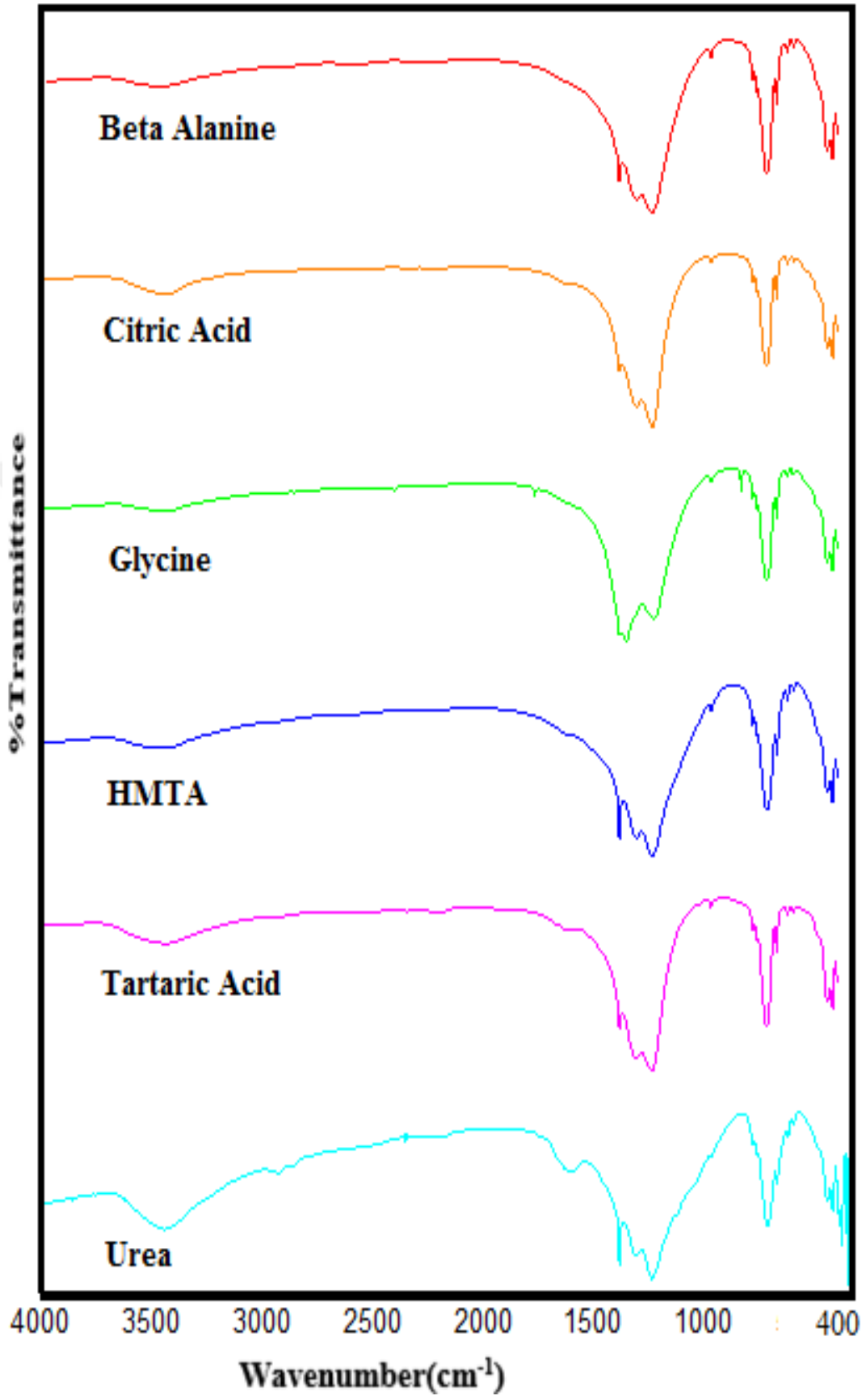

Figure 4.7. FT-IR Spectra of $Zn_3B_2O_6$ at 900°C Using All Fuels

4.1.1.2 X-Ray Diffraction (XRD) Studies

The synthesis of zinc orthoborate, $Zn_3B_2O_6$ with various fuels (urea, glycine, tartaric acid, HMTA, citric acid, and β-Alanine) was completed and the obtained products were heated at different temperatures. Their structural properties were analyzed by X-ray diffraction tecniques. The crystal structure of high-temperature beta-form of $Zn_3B_2O_6$ was first determined by Fayos and Garcia-Blanco in the center-unsymmetrical Ic group, later corrected by Tillmanns and Baur in the center-symmetric group I2/c (25). Recently, the refinement of $Zn_3B_2O_6$ was reported in a standard group C2/c by Chen et al. It was reported that zinc orthoborate ($Zn_3B_2O_6$) exists in two forms, α-$Zn_3B_2O_6$, and β- $Zn_3B_2O_6$. It is stated that the α-$Zn_3B_2O_6$ is formed at low temperature and the β- $Zn_3B_2O_6$ obtained at high temperature.

The XRD analysis was done by comparing International Center for Diffraction Data (ICDD) cards with XRD patterns of the products for the characteristic reflections. The patterns of the obtained products are similar to α-$Zn_3B_2O_6$ and β-$Zn_3B_2O_6$ formation given in the ICDD card No 74-1099 and JCPDS 01-075-3037, respectively as shown in figures 4.8-4.14.

In the examination of XRD patterns, zinc orthoborate was formed as α and β form of zinc orthoborates. The XRD structural analysis of the products obtained at different temperatures were compared with ICDD cards. It showed that β-$Zn_3B_2O_6$ is in a monoclinic and α-$Zn_3B_2O_6$ is in a triclinic crystal structures. The strong and sharp peaks with high intensity in XRD patterns at high temperatures (700-900^{o}C) showed the products are well crystallized and no additional peaks were detected.

In the XRD patterns of as-synthesized products (Figure 4.8), only the product prepared by citric acid fuel formed the amorphous phase, glycine in beta form while the other as-synthesized products form in alpha-form of Zinc orthoborates at lower temperatures, 400^{o}C-600^{o}C. The formation α-$Zn_3B_2O_6$ was confirmed by comparing with the JCPDS 01-075-303.

After further heating at higher temperature, 700^{o}C for an hour the transformation of α-$Zn_3B_2O_6$ to β-$Zn_3B_2O_6$ were observed. The reflectiom lines have great compatability with ICDD card No. 74-1099, which belongs to monoclinic form of $Zn_3B_2O_6$. The single sharp lines at around 2θ=~26º and 28º determine the presences of monoclinic crystal structure of $Zn_3B_2O_6$ (Figure 4.12).

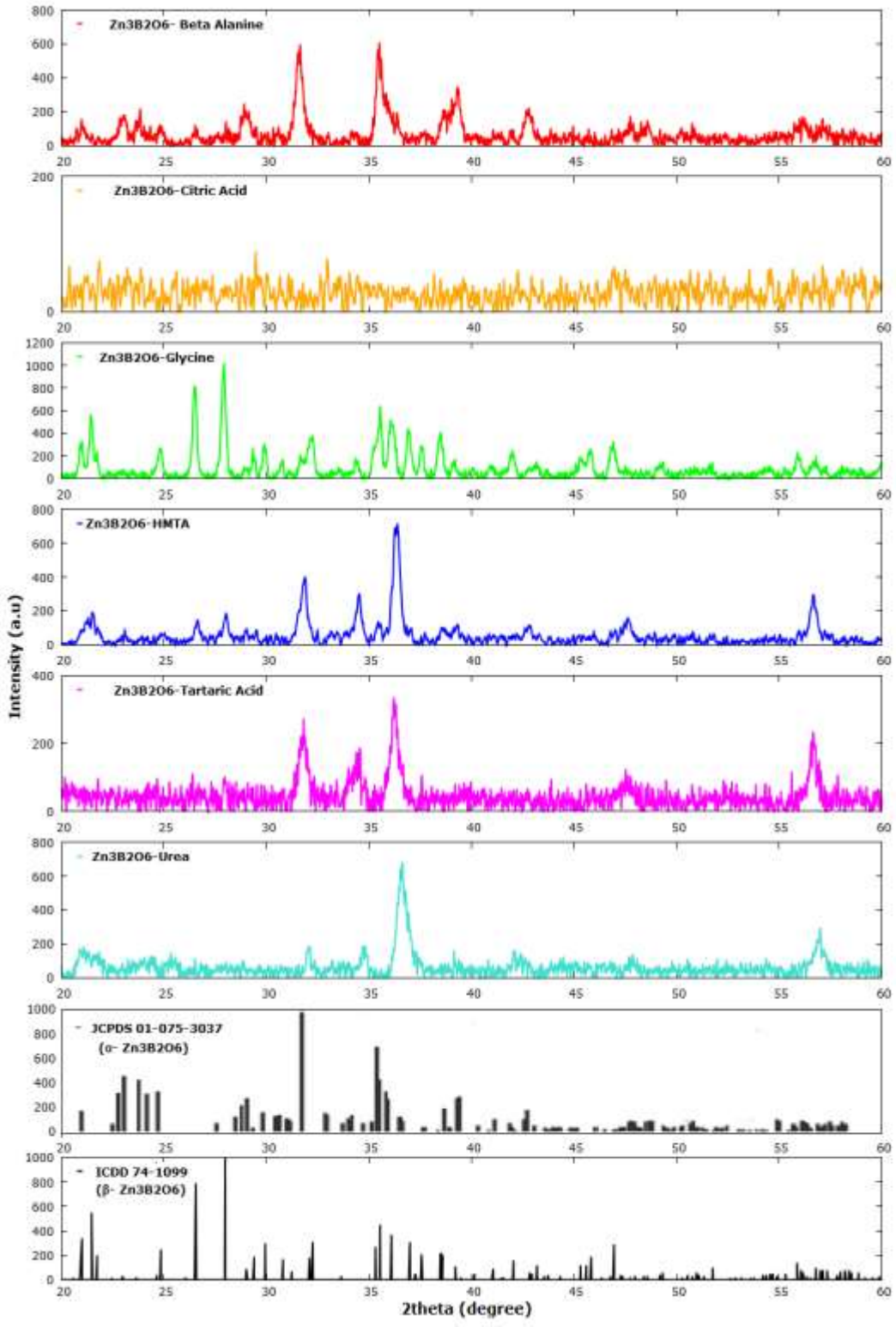

Figure 4.8. XRD Patterns of Synthesis $Zn_3B_2O_6$ with All Fuels

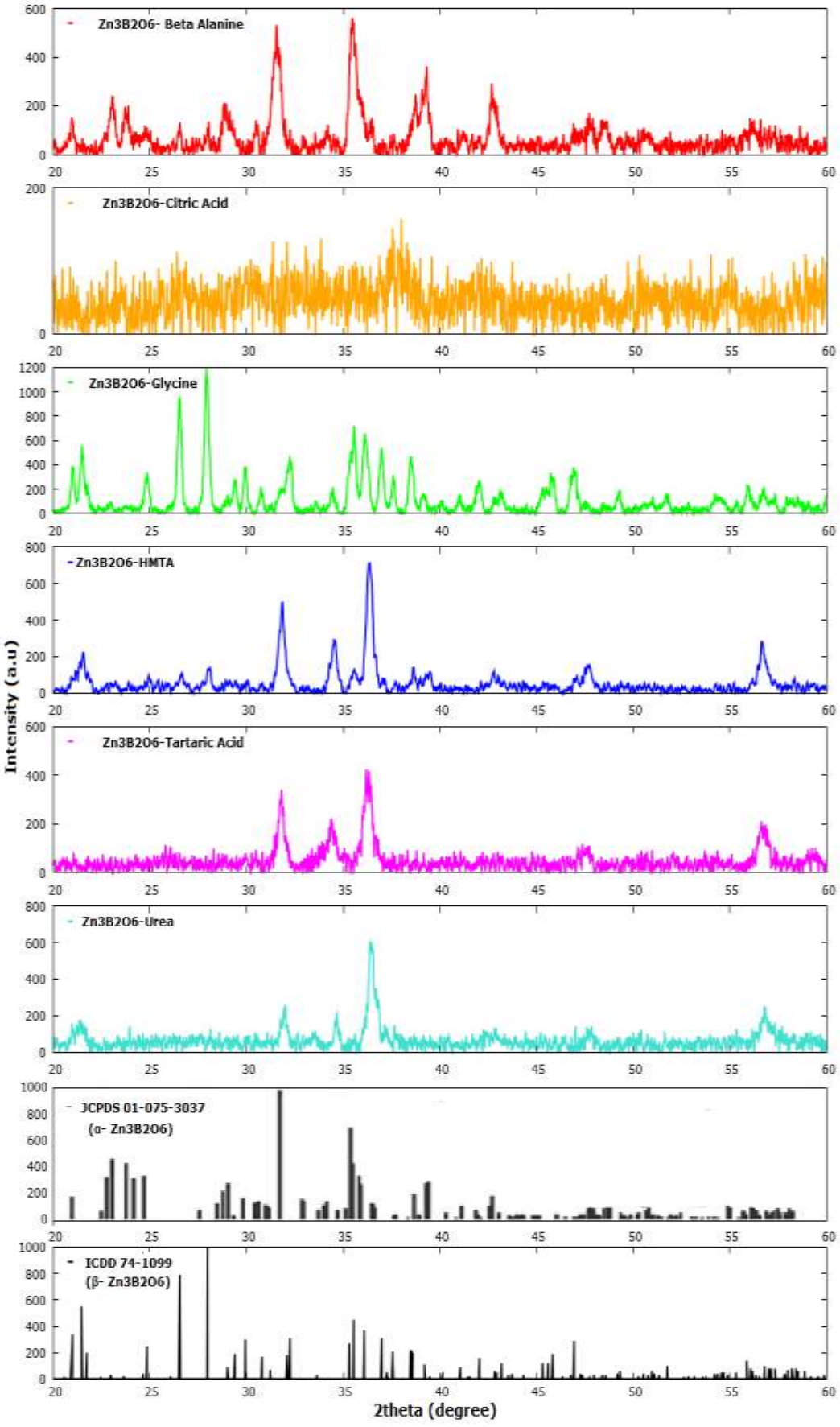

Figure 4.9. XRD Patterns of $Zn_3B_2O_6$ obtained at 400°C with All Fuels

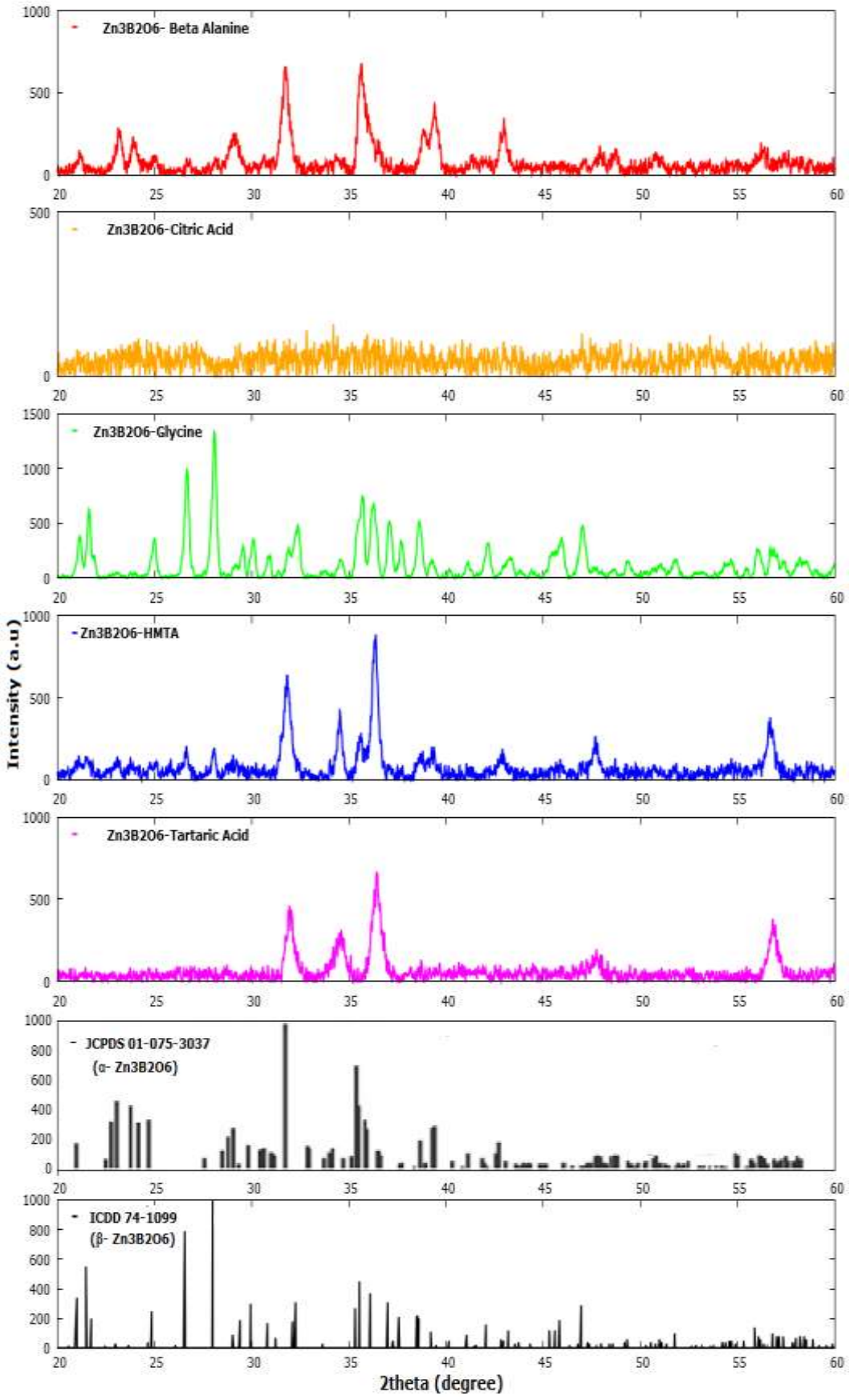

Figure 4.10. XRD Patterns of $Zn_3B_2O_6$ obtained at 500°C with All Fuels

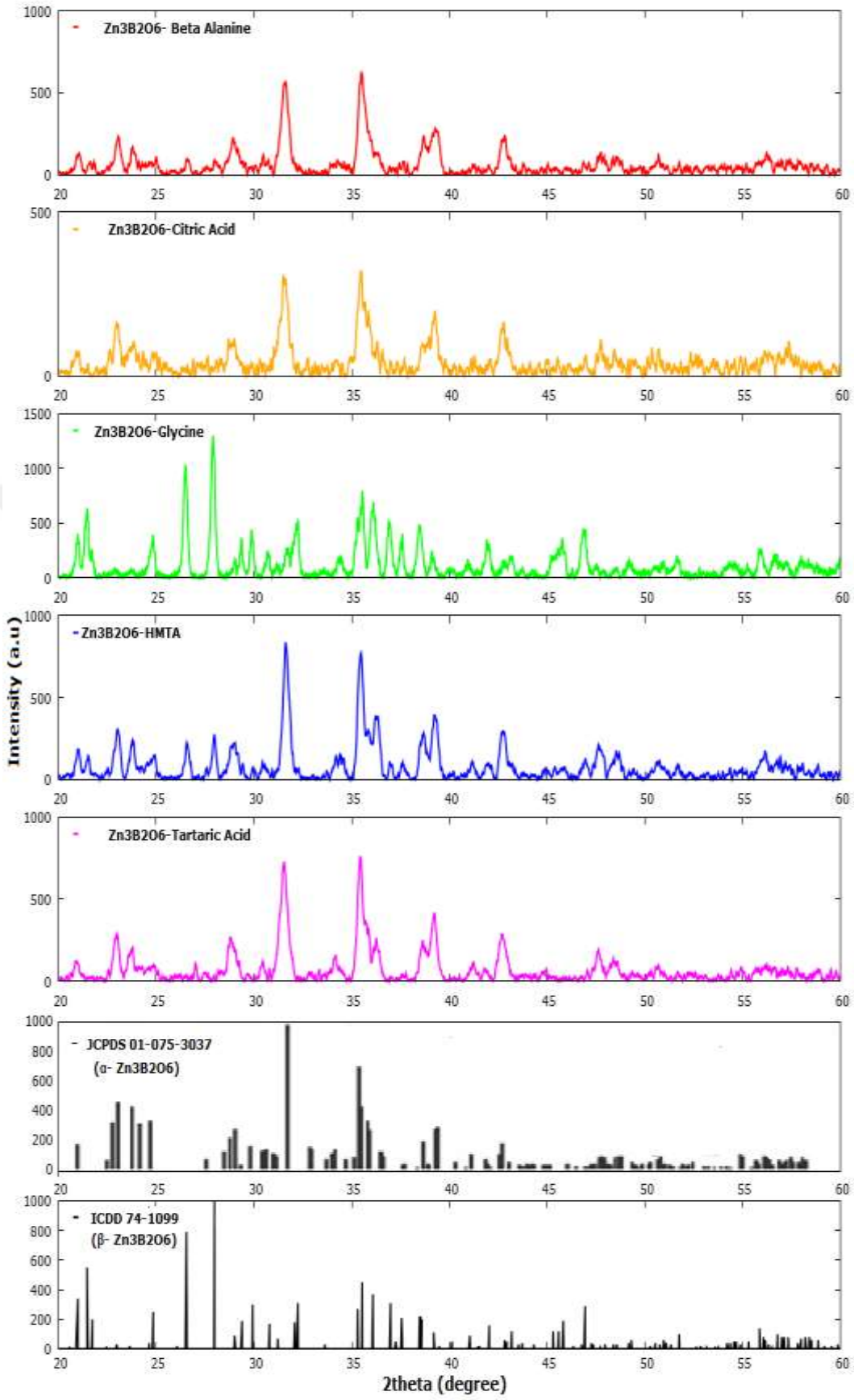

Figure 4.11. XRD Patterns of $Zn_3B_2O_6$ obtained at 600°C with All Fuels

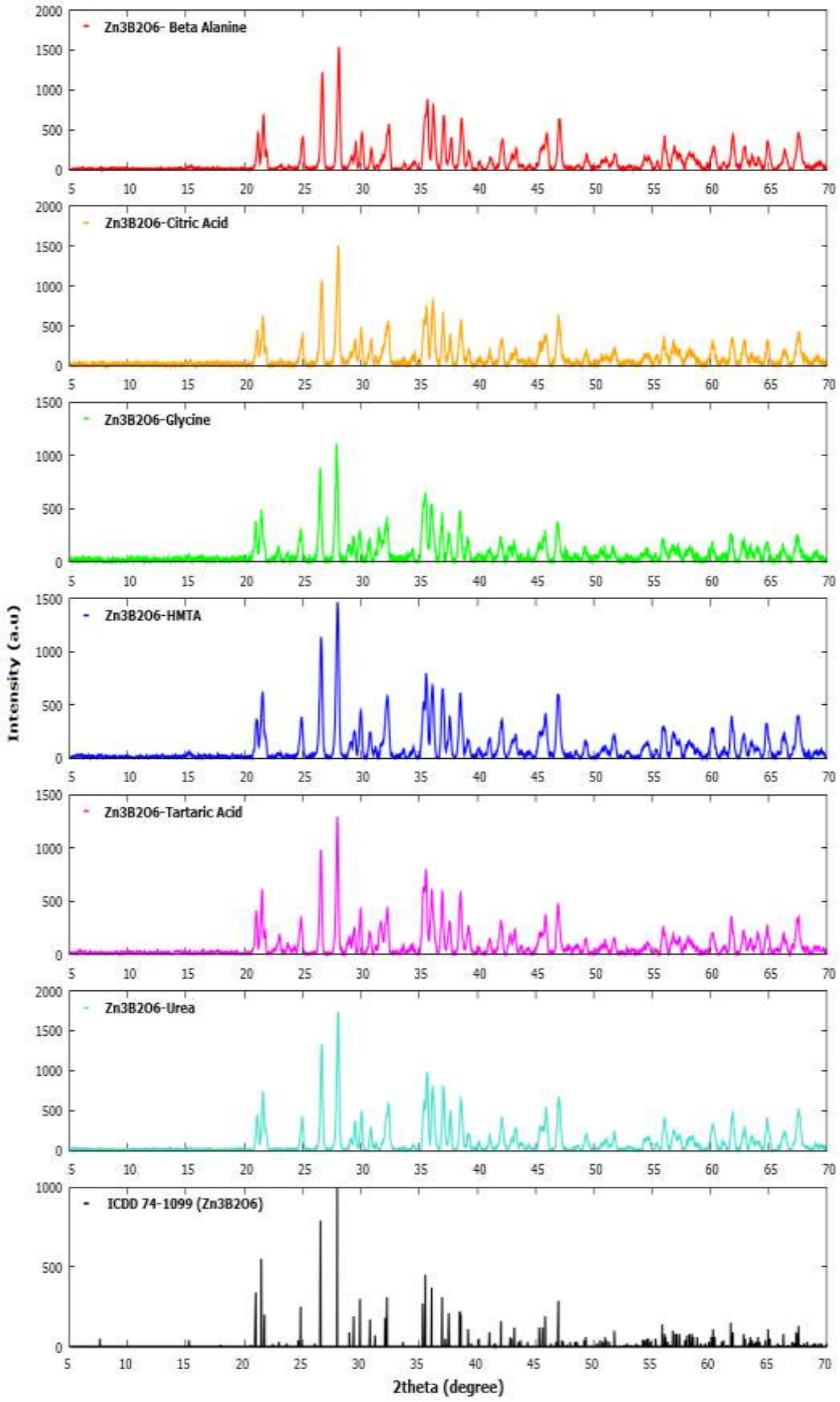

Figure 4.12. XRD Patterns of $Zn_3B_2O_6$ obtained at 700°C with All Fuels

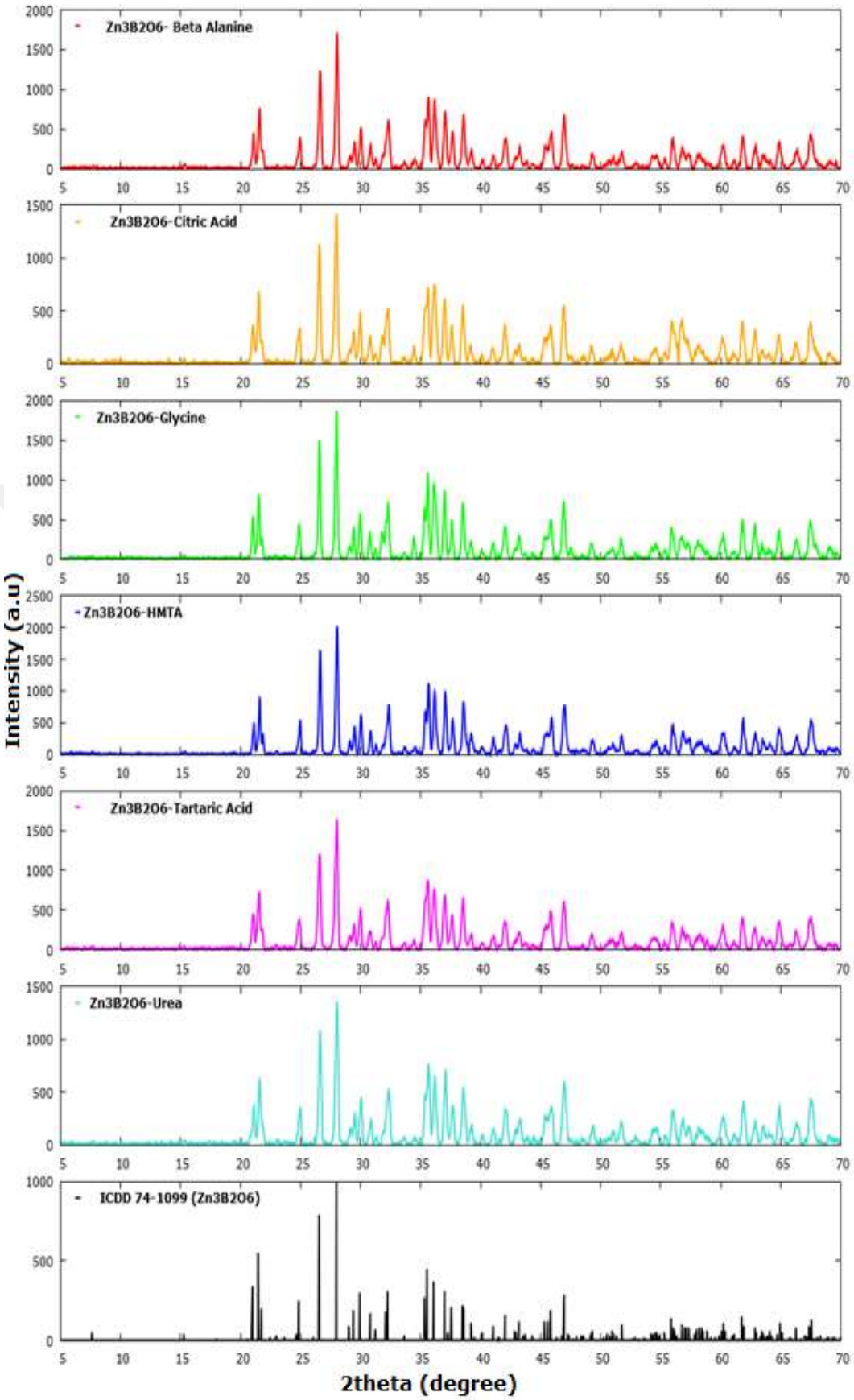

Figure 4.13. XRD Patterns of $Zn_3B_2O_6$ obtained at 800°C with All Fuels

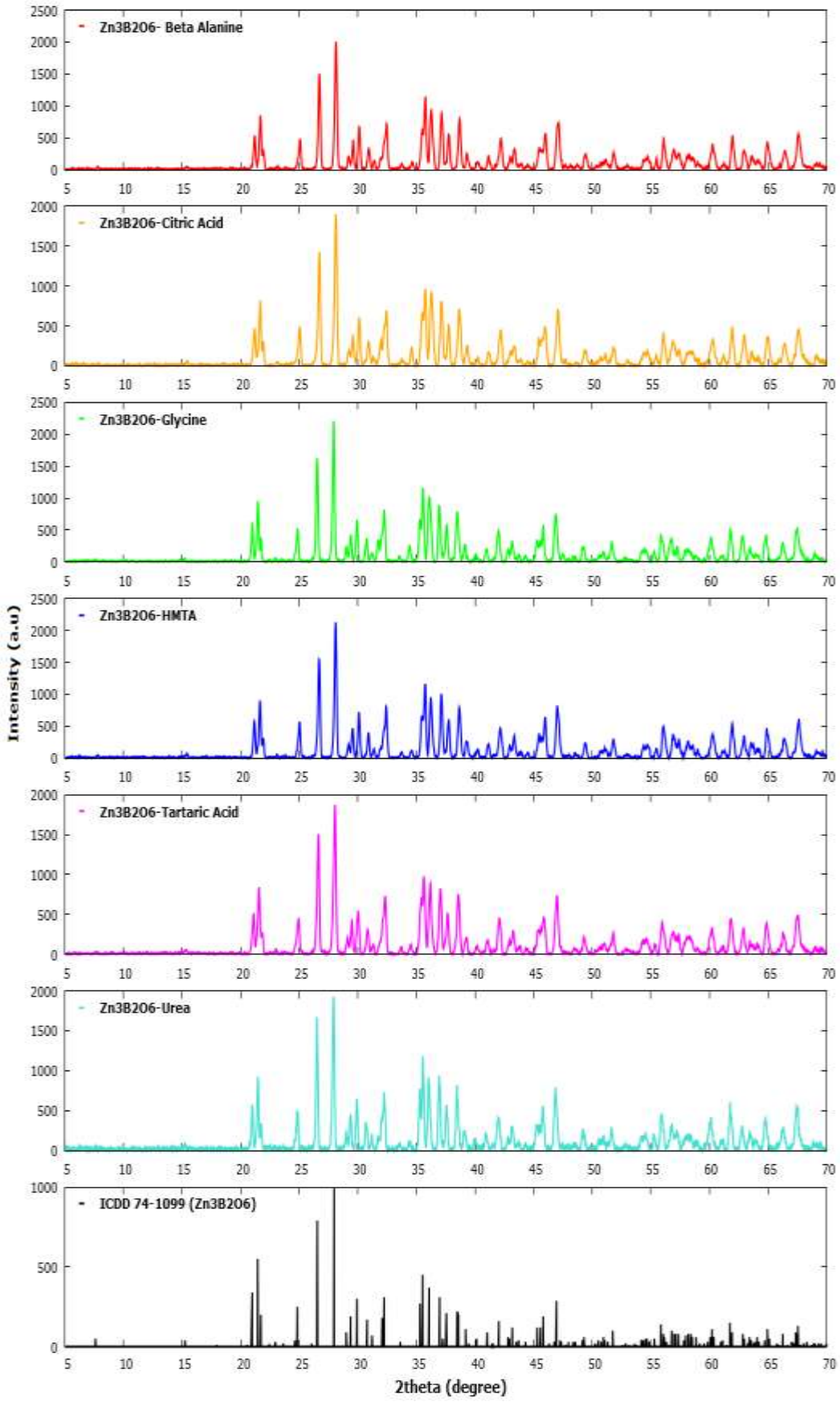

Figure 4.14. XRD Patterns of $Zn_3B_2O_6$ obtained at 900°C with All Fuels

Since the formation of single-phase triclinic α-$Zn_3B_2O_6$ and monoclinic β-Zn3B2O6 were obtained at 600ºC and 700ºC, their crystallite sizes were calculated by using Debye-Scherrer's Equation.

$$D=K\lambda/\beta\cos\theta$$

Where D : average of the crystallite size (nm),

K : factor of shape constant, taken as 0.90

λ : wavelength of the radiation (CuKa) which equal to 1.54056 Å,

β : width of the half intesity of the maximum (radians)

θ : angle of the diffraction (29).

From these crystallite size results formation of nanosized zinc orthoborates were confirmed. It showed that at 600ºC, the crystalite size of products are between 14-24 nm. The obtained products synthesized by urea fuel has the smallest crystallite size among all the obtained products as given in Table 4.7.

Table 4.7. Crystallite size (nm) values of $Zn_3B_2O_6$ at 600 ºC

FUELS	CRYSTALLITE SIZE(nm)
β-Alanine	15.77
Citric Acid	16.85
Glycine	23.68
Hmta	20.53
Tartaric Acid	19.31
Urea	14.44

The crystallite size of the products found at 700ºC give a higher value compared to the one obtained at 600ºC. These results validated the fuels effect on the crystallite size of products. The crystallite sizes are in the range of 22-31 nm with citric acid has the smallest crystallite size, 22.38 nm. The detailed information are given in Table 4.8.

Table 4.8. Crystallite size (nm) values of $Zn_3B_2O_6$ at 700 °C

FUELS	CRYSTALLITE SIZE(nm)
ß-Alanine	27.22
Citric Acid	22.38
Glycine	22.44
Hmta	27.35
Tartaric Acid	30.48
Urea	30.28

To determine the temperature effect on the crystallite size, the calculations were also done for the products synthesized by urea fuel. The results are between 11-35 nm and show a direct relation as that the crystallite size increases with respect to increase of heating temperature (Table 4.9).

Table 4.9. Crystallite size (nm) values of $Zn_3B_2O_6$ synthesized by urea fuel

TEMPERATURE	CRYSTALLITE SIZE(nm)
Synthesis	11.45
400	12.29
500	13.59
600	14.44
700	30.28
800	30.31
900	34.55

4.1.1.3 The UV-Visible Spectroscopy Studies

The effect of annealing temperature and fuels on the optical properties of the obtained products were examined. The absorbance and the reflactance of the alpha and beta forms of zinc orthoborates acquired at 600°C and 700°C was presented below, respectively. The spectra recorded at the range between 900-200 nm and the data were plotted using the UV WinLab program where the behavior of light radiated by products could also be determined.

The Table 4.10 and 4.11 are represent the absorbance and also reflectance data of the products at each temperature. It is showed that by changing the fuel type, the spectra are blue shifted as they shifted from longer wavelegth to shorter wavelength from citric acid, HMTA, urea, tartaric acid, glycine and beta-alanine

consecutively. Whereas at 700ºC the order from longer to shorter wavelegth are urea, HMTA, tartaric acid, citric acid, b-alanine and glycine. These phenomenon has proven that different type of fuels do affect the optical properties at the same temperatures. More additions, the spectra are also blue shifted and red shifted with higher temperatures depends on the applied fuels, as shown in Table 4.10 and 4.11

Table 4.10. The absorbance and wavelength values of $Zn_3B_2O_6$

$Zn_3B_2O_6$	**600ºC**		**700ºC**	
	Absorbance (A)	**Wavelength (nm)**	**Absorbance (A)**	**Wavelength (nm)**
Beta Alanine	0.51	336.25	0.47	363.42
Glycine	0.51	363.78	0.44	354.68
HMTA	0.40	366.24	0.40	368.51
Citric Acid	0.69	385.42	0.43	364.29
Tartaric Acid	0.54	365.05	0.34	366.83
Urea	0.28	365.69	0.35	368.87

Table 4.11. The Reflectance and wavelength values of $Zn_3B_2O_6$

$Zn_3B_2O_6$	**600ºC**		**700ºC**	
	Reflectance (%R)	**Wavelength (nm)**	**Reflectance (%R)**	**Wavelength (nm)**
Beta Alanine	54.09	366.25	29.82	364.05
Glycine	32.41	366.24	37.37	355.14
HMTA	38.95	365.69	41.07	368.73
Citric Acid	18.89	382.28	35.34	363.79
Tartaric Acid	29.79	367.46	44.88	367.33
Urea	54.09	366.25	45.45	371.17

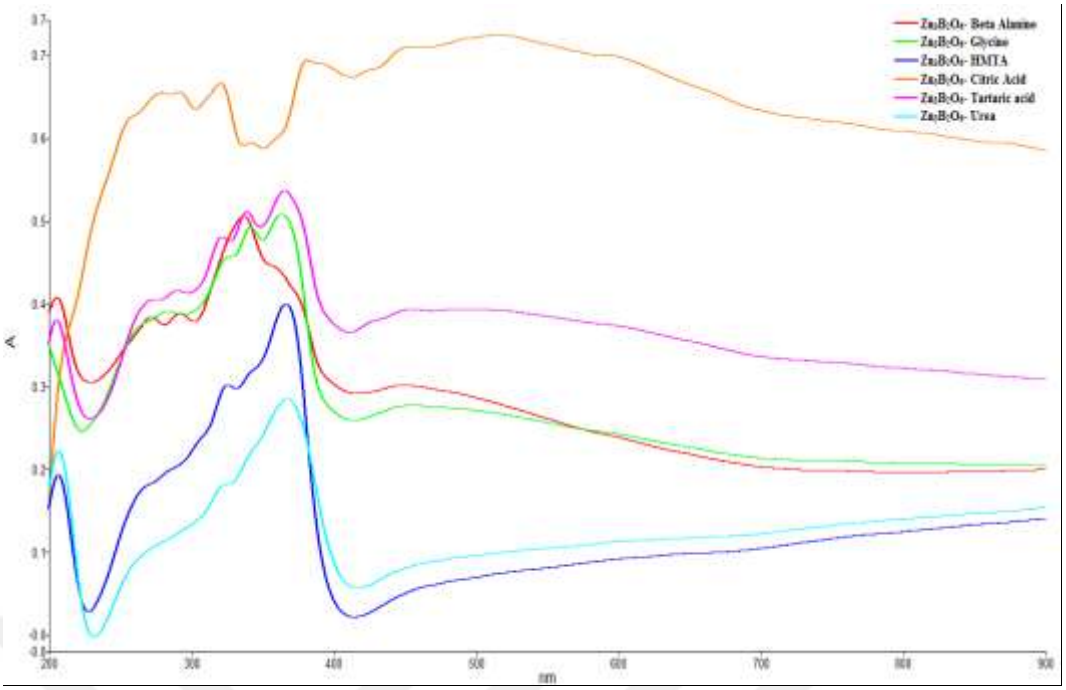

Figure 4.15. The absorbance spectra of $Zn_3B_2O_6$ obtained at 600°C with All Fuels

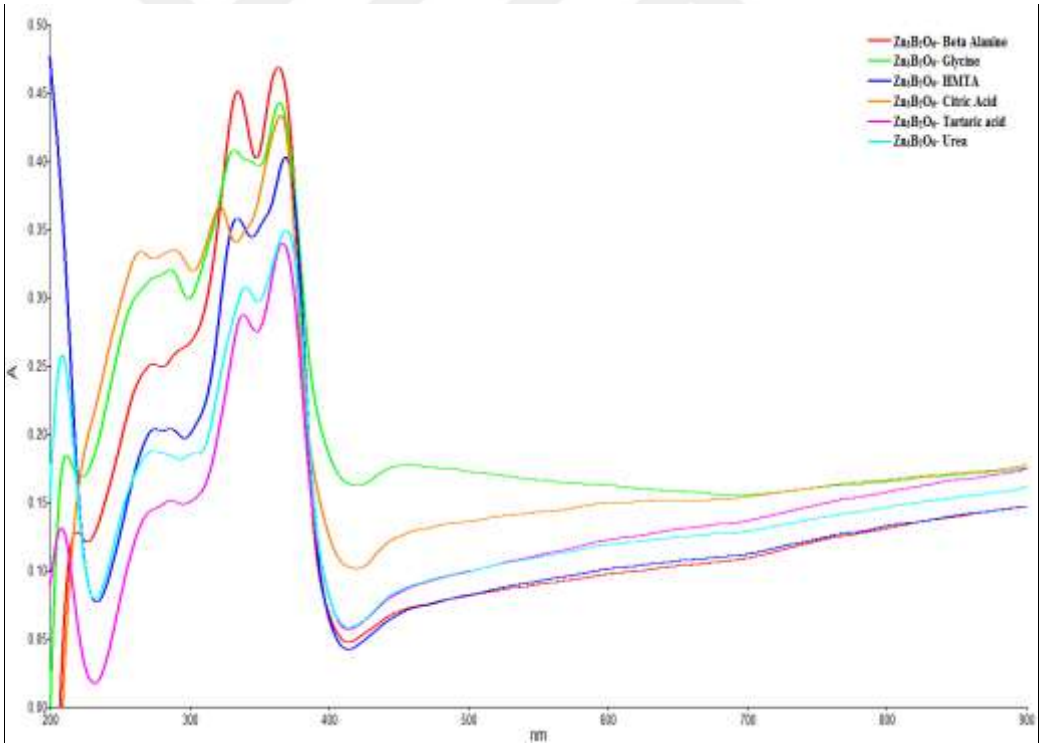

Figure 4.16. The absorbance spectra of $Zn_3B_2O_6$ obtained at 700°C with All Fuels

The reflectance values along with its wavelength are listed in Table 4.11 Similar to the absorbance spectra, two main peaks are observed at around 300-400 nm as shown in Figure 4.17 and 4.18.

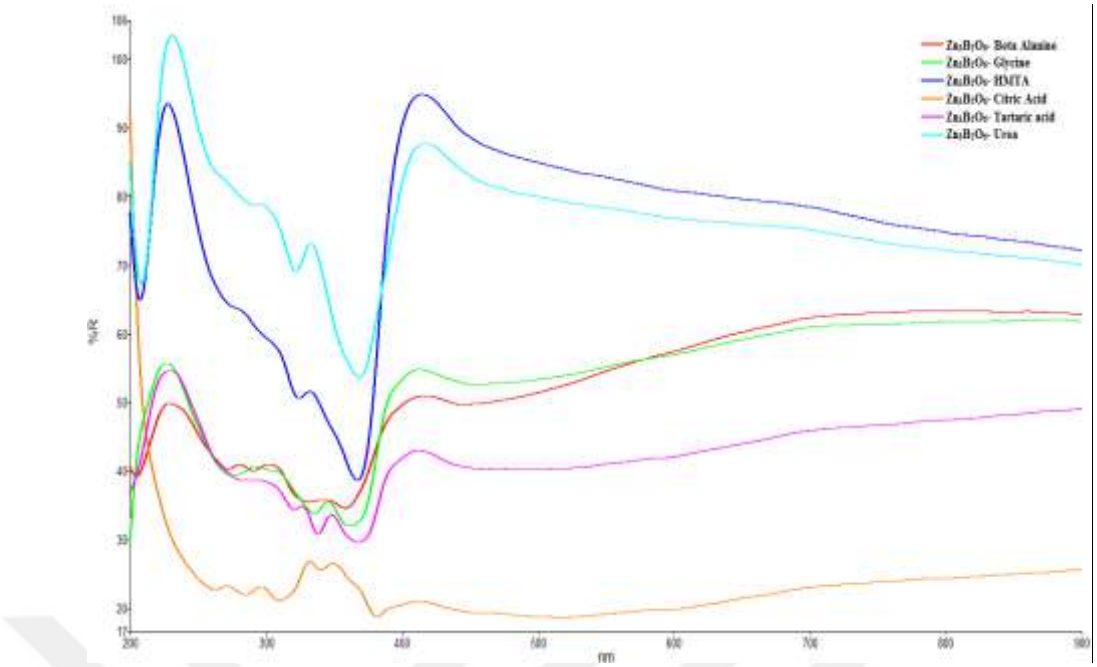

Figure 4.17. The reflectance spectra of $Zn_3B_2O_6$ obtained at 600°C with All Fuels

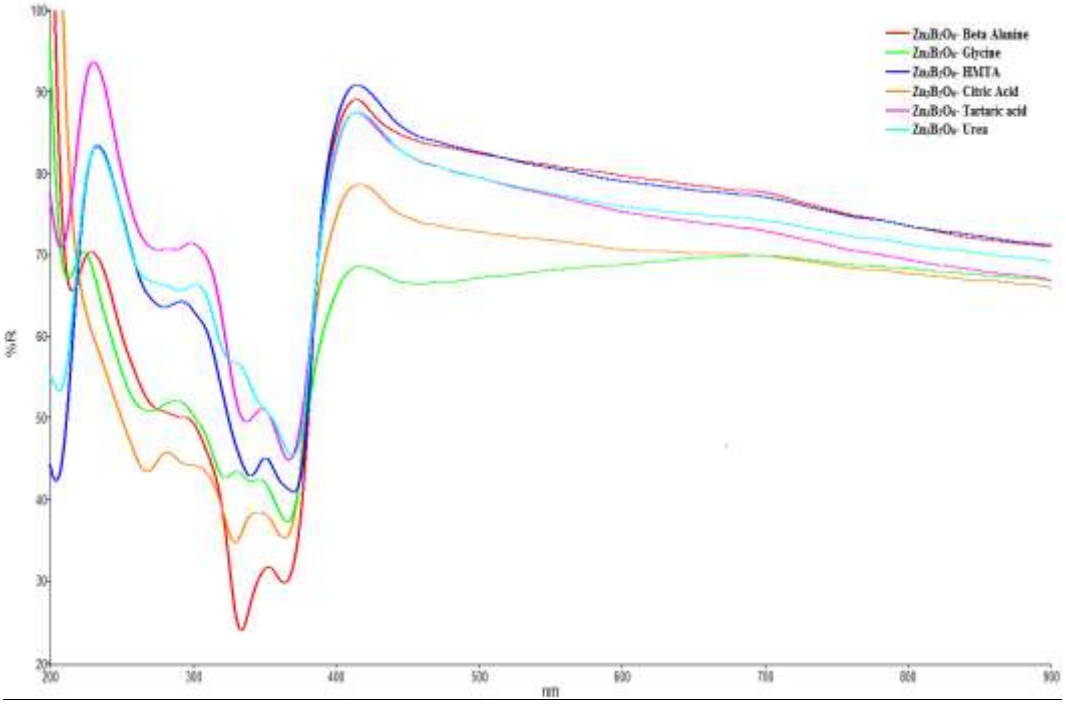

Figure 4.18. The reflectance spectra of $Zn_3B_2O_6$ obtained at 700°C with All Fuels

The effect of heating temperatures on the change of wavelength is also examined by using the data given by product obtained with urea fuel. The spectra are showed to be back and fort from lower to higher wavelength and vice versa. But it can be seen that the wavelength are red shifted from ~357.07 nm which belongs

to the as-prepared products to 368.87 nm that assigned to single phase beta zinc orthoborate obtained at 700ºC (Table 4.12).

Table 4.12. The Reflectance, Absorbance and wavelength values of $Zn_3B_2O_6$

$Zn_3B_2O_6$ (UREA)	**A/Wavelength(nm)**	**%R/Wavelength(nm)**
Synthesis	0.25/357.07	57.73/366.85
400ºC	0.33/355.70	45.96/372.26
500 ºC	0.34/362.40	45.14/363.21
600 ºC	0.29/357.33	54.09/355.25
700 ºC	0.35/368.87	45.94/371.71
800 ºC	0.28/358.35	51.41/359.76
900 ºC	0.33/371.09	48.40/366.78

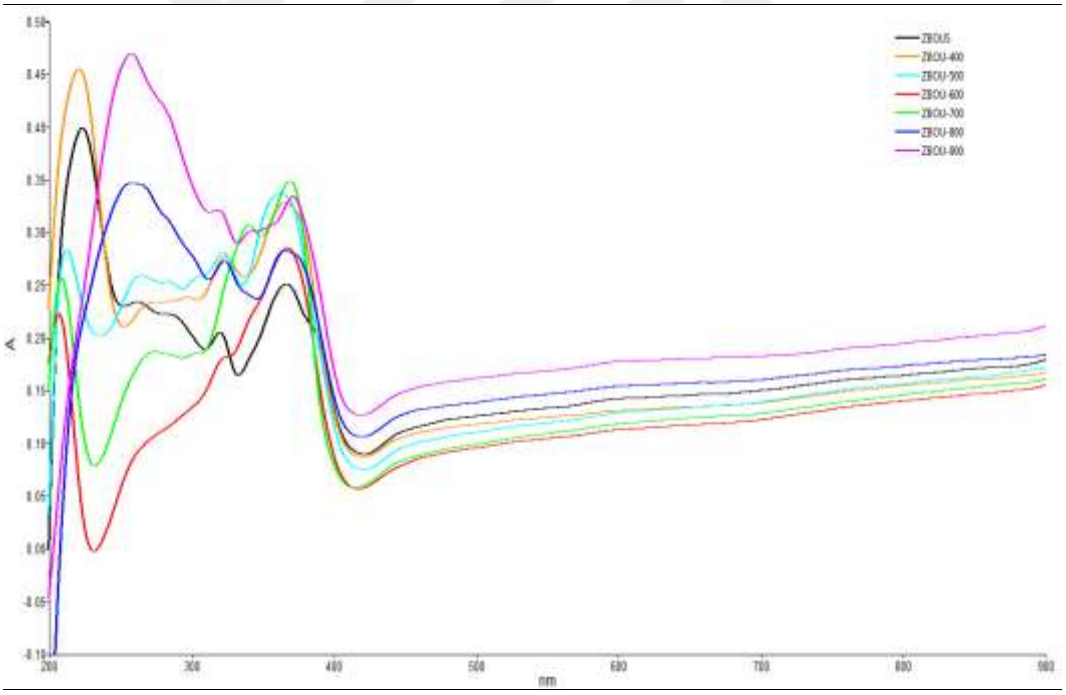

Figure 4.19. The absorbance spectra of $Zn_3B_2O_6$ with urea fuel at all temperatures

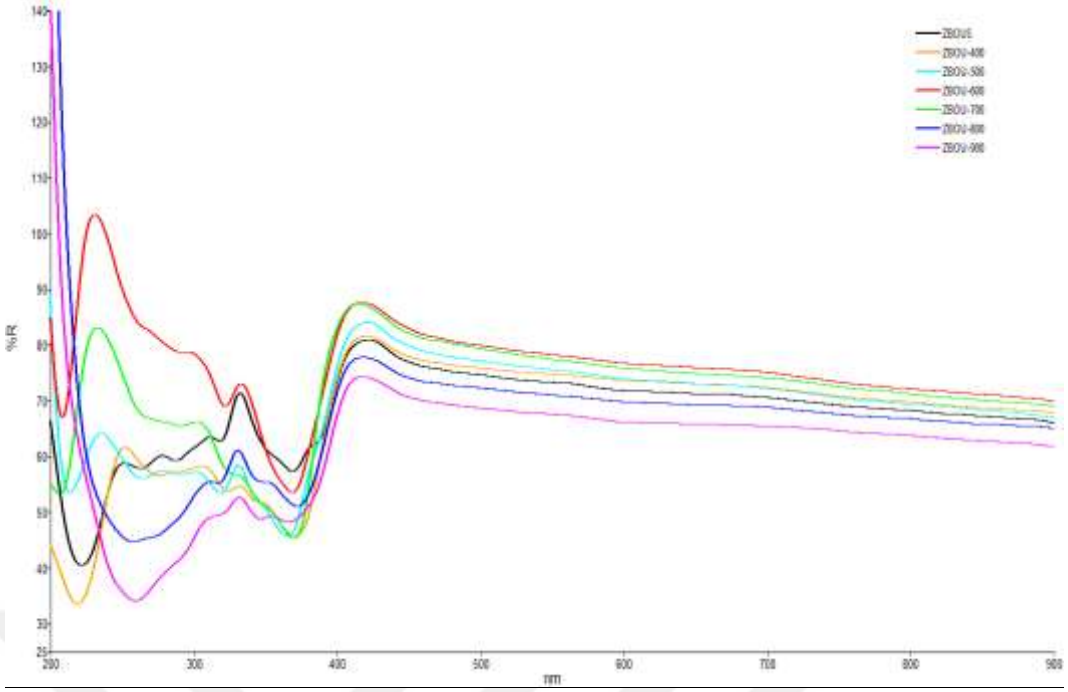

Figure 4.20. The reflectance spectra of $Zn_3B_2O_6$ with urea fuel at all temperatures

5. CONCLUSIONS AND RECOMMENDATIONS

In this present study, $Zn_3B_2O_6$ nanosized were successfully synthesized by a simple, cost effective, and time performance Solution Combustion Synthesis (SCS) method. The single-phase synthesis products were obtained in brief reaction time and low synthesis temperature.

In the analysis of XRD, the formation of α and β form of zinc orthoborates were determined. According to the XRD pattern analysis, the alpha-zinc orthoborate was attained at lower temperatures, 400-600^oC in triclinic form for all fuels except glycine fuel while the transformation of alpha to beta form of zinc orthoborate with monoclinic crystal structure was observed at higher temperature, 700^oC. The single phase of β-$Zn_3B_2O_6$ were successfully obtained in which its diffraction lines are well coincided with reference pattern given by ICDD No.74-1099.

The crystallite sizes of of α and β forms of zinc orthoborates were calculated by using Debye-Scherrer's equations. The results showed that the obtained products were in nano scale in the range of 14-24 nm for alpha and 22-31 nm for beta borate at 600^oC and 700^oC, respectively. The temperature effect on the crystallite size was also examined using urea as fuel which showed the direct relation with the temperature as the higher temperature the bigger the crystallite sizes obtained.

The analysis of FT-IR spectra of zinc orthoborate in alpha and beta forms showed that the bending BO_3 vibration is between 695 and 720 cm^{-1}, symmetric stretching of BO_3 vibration were detected at around 1010 and 1065 cm^{-1}, while the bands in the range of 1220 and 1245 cm^{-1} were assigned to the asymmetric stretching of BO_3 vibration.

The optical properties of products have also been examined and it is showed that the spectra are detected at the range of 200-400 nm. The spectra acquired at 600^oC which belong to alpha zinc orthoborates are blue-shifted in order of citric acid, HMTA, urea, tartaric acid, glycine and beta-alanine while the beta form of zinc orthoborates obtained at 700^oC are also blue-shifted but in different arrangement, namely urea, HMTA, tartaric acid, citric acid, b-alanine and glycine. The red shift was observed by urea fuels for the as-synthesized product which has shorter wavelength than the one obtained at 700^oC.

6. REFERENCES

Vancouver citation system was used in this thesis.

1. Greenwood NN, Earnshaw A. Chemistry of the elements. 2nd ed. Oxford: Butterworth Heinemann; 1972.

2. Sümer G. Boron compounds, II.International Boron Symposium, 23-25 September 2004, Eskişehir, Turkey, 153-164

3. Demiral Kurtuluş F, Güler H. Synthesis of Some Metal Containing Borate and Boron Phosphate Compounds by Solid-State Methods. Journal of Balikesir University Institute of Natural and Applied Sciences. 2003; 5(1): 141-152

4. Boron[Internet].[cited 2022 Nov 16]https://www.priyamstudycentre.com/2020/11/boron.html.

5. Yılmaz A. Her Derde Deva Hazinemiz Bor. Journal of Science and Technology. 2002; 414: 39-48.

6. Chatterjee KK. Uses of metals and metallic minerals. New Delhi: New Age International Publishers; 2007

7. Boron Element [Internet].[cited 2022 Nov 18]. Available from: https://boren.tenmak.gov.tr/tr/calisma-alanlari/bor-elementi.html.

8. Cengiz E. Özelleştirmenin Odağındaki Bor, 1.International Boron Symposium, 3-4 October 2002, Kütahya, Turkey, 39-42.

9. Boron Element [Internet].[cited 2022 Nov 18]. Available from: http://w3.balikesir.edu.tr/~hguler/bor_kimyasi.htm.

10. Yiğitbaşıoğlu H. Türkiye için Önemli Bir Maden Bor. Journal of Geographical Sciences. 2004; 2(2): 13-25.

11. History [Internet].[cited 2022 Nov 18]. Available from: https://boren.tenmak.gov.tr/tr/calisma-alanlari/tarihce.html

12. Beatty R. The elements boron. New York: Marshall Cavendish Benchmark; 2006

13. Boron Minerals [Internet]. [cited 202 Nov 20]. Available from: https://www.etimaden.gov.tr/bor-mineralleri.

14. Boron in the Turkey[Internet].[cited 2022 Nov 21]. Available from: https://www.etimaden.gov.tr/en/boron-in-turkey

15. Boron in the World[Internet].[cited 2022 Nov 21]. Available from: https://www.etimaden.gov.tr/en/boron-in-world

16. Boron[Internet].[cited 2022 Nov 21]. Available from: https://enerji.gov.tr/infobank-naturalresources-boron

17. Eltepe HE, Balköse D, Ülkü S. Effect of Temperature and Time on Zinc Borate Species Formed from Zinc Oxide and Boric Acid in Aqueous Medium. Industrial & Engineering Chemistry Research. 2007; 46(8):2367–2371.

18. Briggs M. Boron Oxides, Boric Acid, and Borates. Kirk-Othmer Encyclopedia of Chemical Technology. 2001; 4: 241-294

19. Lee JD. A New Concise Inorganic Chemistry. 3rd. ed. London: English Language Book Society; 1977

20. Weir CE. Infrared Spectra of the Hydrated Borates. A. Physics and Chemistry. 1966; 70A (2):153-164.

21. Gül E. Synthesis and characterization of novel-mixed- metal-orthoborates.Msc Thesis. Abant İzzet Baysal University

22. Eltepe HE, Balköse D, Ülkü S. Effect of Temperature and Time on Zinc Borate Species Formed from Zinc Oxide and Boric Acid in Aqueous Medium. Industrial & Engineering Chemistry Research. 2007; 46(8):2367–2371.

23. Samyn F, Bourbigot S, Duquesne S, Delobel R. Effect Of Zinc Borate On The Thermal Degradation Of Ammonium Polyphosphate. Thermochimica Acta. 2007; 456(2):134–144.

24. Shen KK, Kochesfahani S, Jouffret F. Zinc borates as multifunctional polymer additives. Polymers For Advanced Technologıes. 2008; 19(6):469–474.

25. Schubert DM. Zinc Borate. United States Borax & Chemical Corporation. 1993; Patent Cooperation Treaty, No: WO 93/10045

26. Chen X, Xue H, Chang X, Zhang L , Zhao Y, Zuo J et al. Syntheses and crystal structures of the α- and ß-forms of zinc orthoborate, $Zn_3B_2O_6$. Alloys and Compounds. 2006; 425(1-2):96-100.

27. Bobkova NM, Khotko SA. Structure Of Zinc-Borate Low Melting Glasses Derived From IR Spectroscopy Data. Journal of App. Spectroscopy. 2005; 72(6): 853–857.

28. Zinc Borate[Internet].[cited 2022 Nov 29]. Available from: https://www.etimaden.gov.tr/en/zinc-borate.

29. Chen DG, Cheng WD, Wu DS, Zhang H, Zhang YC, Gong YJ, Kan ZG. Syntheses, band structures and optical properties of $Zn_3B_2O_6$ and $KZn_4B_3O_9$. Solid State Sciences. 2005 Feb;7(2): 179-188.

30. Hirokazu M, Takahiro U, Yoshihiro T, Takumi F. Fabrication of surface crystallized glasses with α-$Zn_3B_2O_6$ and their optical property. Journal of Non-Crystalline Solids. 2010 Oct;356(44-49):2689-2692.

31. Xin GW, Hong W, Yue HC, Di Z. Synthesis and Microwave Dielectric Properties of $Zn_3B_2O_6$ Ceramics for Substrate Application. 2012 Jun;95(6):1777-2073.

32. Sarma GVSS, Chava VR, Vattikuti SVP, Chava RK, Narayana Murthy P, Ravikumar RVSSN. Spectral investigations of Mn^{2+} doped $Zn_3(BO_3)_2$ nanopowder. Journal of Molecular Structure. 2013 Sep 24;1048:64-68.

33. Yurong S, Yan W, Meidan Q, Ge Z, Yuhua W. Structure, photoluminescent and cathodoluminescent properties of a rare-earth free red emitting β-$Zn_3B_2O_6$:Mn^{2+} phosphor. Dalton Transactions 2014;43(6):2418-2423.

34. Jaesool S, Chava VR, Sarma GVSS, Narayana Murthy P, Ravikumar RVSSN. Effect of Co^{2+} and Ni^{2+} doped zinc borate nano crystalline powders by co-precipitation method. Spectrochimica Acta Part A: Molecular and Biomolecular Spectroscopy 2015 May 5;142:279-285.

35. Chava VR, Sarma GVSS, Ravikumar RVSSN, Jaesool S. Synthesis and spectroscopic characterizations of copper ions doped zinc borate nanoparticles. Optik 2016;127(10):4536–4540.

36. Kamazanil MM, Rahmatolahzadeh R, Shobeiri SA. Facile sol–gel auto-combustion synthesis of β-$Zn_3B_2O_6$ nanoparticles:optical and photocatalytic studies. Journal of Materials Science: Materials in Electronics 2017;28(23):17961-17967.

37. Zhou D, Yan G, Zhang W, Lin J, Qiu K. Synthesis and luminescence properties of $Zn_3B_2O_6:Eu^{3+}$, Li^+ red-emitting phosphor for white LEDs. Ferroelectrics 2018 Jun 14;528(1):114-121.

38. Kui J, Hongtao Y, Lin Y, Guangliang X. Ultra-Low Temperature Sintering and Dielectric Properties of SiO_2-Filled Glass Composites. Journal of the American Ceramic Society 2013;96 (11):3563–3568.

39. Zhang Q ,Tang X, Zhong M, Li Y, Jing Y, Su H. Bond characteristics and microwave dielectric properties of high-Q materials in li-doped $Zn_3B_2O_6$ systems. Journal of the American Ceramic Society 2021 May;104(5):2102-2115.

40. Peng R, Li Y, Su H , Lu Y, Yu C, Yu G, et al. A detailed study of the substitution mechanism for improved zinc-borate: High-performance and its crystal structure variation. Journal of Materials Research and Technology 2021;12:1360-1367.

41. Li C, Liu Y, Chi M, Luo X, Liu B, Mao M , et al. ULTCC post-annealing cold sintering densification process, microwave dielectric properties of $Zn_3B_2O_6$ ceramics. Materials Today Communications 2022;33:104997.

42. Kopp Alves A, Bergmann CP, Berutti FA. Introduction, in: Novel Synthesis and Characterization of Nanostructured Materials. Springer Berlin Heidelberg. Berlin. pp. 1–9..2013

43. Li F, Ran J, Jaroniec, Qiao SZ. Solution combustion synthesis of metal oxide nanomaterials for energy storage and conversion.Nanoscale. 2015;45